Dynamics of acoustic impedance matching layers in contactless ultrasonic power transfer systems

IOP Publishing Smart Materials and Structures
Smart Mater. Struct. **29** (2020) 035037 (20pp) https://doi.org/10.1088/1361-665X/ab6fe5

Dynamics of acoustic impedance matching layers in contactless ultrasonic power transfer systems

Marjan Bakhtiari-Nejad[1], **Muhammad R Hajj**[2] **and Shima Shahab**[1,3]

[1] Department of Biomedical Engineering and Mechanics, Virginia Tech, Blacksburg, VA 24061, United States of America
[2] Davidson laboratory, Department of Civil, Environmental and Ocean Engineering, Stevens Institute of Technology, Hoboken, NJ 07030, United States of America
[3] Department of Mechanical Engineering, Virginia Tech, Blacksburg, VA 24061, United States of America

E-mail: sshahab@vt.edu

Received 7 July 2019, revised 12 November 2019
Accepted for publication 24 January 2020
Published 19 February 2020

Abstract

The acoustic impedance mismatch between transducer materials and medium in ultrasonic power transfer systems narrows the transduction bandwidth and causes losses through the back reflection of progressive pressure waves at the boundary between the transducers and medium. Capturing both resonances and losses due to impedance mismatch of interwoven elements is essential for advancing the development of these systems. We present a unified approach, based on the multiplication of a sequence of transfer matrices, to determine an equivalent acoustic impedance. The analytical model couples the properties of the transmitter and receiver with multiple matching layers and a single classical quarter-wave layer in controlled setups with the objective of minimizing reflections through acoustic impedance mismatch alleviation. Losses due to ultrasonic attenuation in the material layers and medium are also considered. The acoustic field at the receiver location constitutes the input to the coupled electro-elastic equations of the fluid-loaded and electrically-loaded piezoelectric receiver. Experiments are performed to identify the input acoustic pressure from a cylindrical transmitter to a receiver disk operating in the 33-mode of piezoelectricity. The results show significant enhancements in terms of the receiver's electrical power output when implementing a two-layer matching structure. We present the results showing non-dimensional wave number variations versus characteristic impedance, which can be used to calculate the materials' thicknesses for acoustically matching ultrasonic power transfer systems to an acoustic medium of interest at any desired resonant frequency while considering any type of glue or epoxy as the bonding layer. The derived physical models facilitate the development of high-fidelity matched systems with enhanced contactless power transmission.

Keywords: acoustic impedance matching layers, ultrasonic power transfer, piezoelectric transducers, ultrasonics

(Some figures may appear in colour only in the online journal)

1. Introduction

Ultrasonic power transfer (UPT) is based on transferring energy using acoustic waves generated and received by piezoelectric transducers. The sound wave is generated by a transmitter and then transferred through an acoustic medium such as water [1, 2], air [3, 4], human tissue [5, 6] or solid wall [7, 8] to a receiver, which in turn converts the mechanical strain induced by the incident acoustic waves to electricity that can be delivered to an electrical load [1]. A review highlighting major advancements in UPT is presented by Roes *et al* [9]. Various UPT concepts using piezoelectric

transduction include: (i) an array of receivers excited by a pulsating sphere, i.e., spherical acoustic transmitter [1, 2], (ii) cylindrical source-cylindrical receiver combination in a separate domain (e.g., as in transcutaneous UPT [5, 10]), (iii) enhanced power transfer by focusing of the source using a high-intensity focused ultrasound (HIFU) transducer [11] or passive acoustic holograms (lenses) when illuminated with an acoustic source such as a PZT (lead zirconate titanate) disk as the active element to generate a desired pressure pattern [12, 13], (iv) identification of electro-elastic nonlinearities in UPT systems [14], and (v) enhanced power transfer by acoustic impedance matching of the transmitter and receiver disks to the medium, which is the scope of this work. The proposed scenarios for performance enhancement and frequency bandwidth improvement of UPT systems mainly include focusing of the transmitted acoustic energy in space and alleviating impedance mismatch issues [2]. To improve the efficiency of UPT systems, minimizing the acoustic losses due to the reflection of acoustic waves must be considered. The characteristic impedance, which depends on the density and speed of sound in materials, is one of the most significant acoustical parameters in acoustic power transmission. Because the characteristic impedance of piezoelectric (PZT) transducers is much larger than that of acoustic media, i.e., air, liquid, human tissue or solid wall, the transducers need to be acoustically matched. The acoustic impedance mismatch between the PZT elements and the acoustic medium results in (i) a narrow frequency bandwidth [15–17] and (ii) significant losses through back reflection of the incident pressure waves at the boundary between the PZT and the medium [18]. For example, the pressure reflection coefficient for a soft tissue is 0.9 which means that only 10% of the incident wave is captured by the piezoelectric receiver. To alleviate the acoustic impedance mismatch, intermediate materials, called acoustic impedance matching layers are used [19]. Such layers are bonded to the front side of the transducer face.

Several theoretical and experimental investigations considered the effects of implementing a single or multiple quarter-wavelength layers in the design of piezoelectric transducers [15–18, 20–33]. Materials ranging from metals, ceramics or composites, such as silver, titanium, and glass to polymers or plastics, such as parylene and acrylic have been used as matching layers. In a few studies [34–37], a mass-spring matching approach was proposed to determine layer thicknesses in which multi-layer polymer-metal structures such as a double structure of PVDF-copper and polyimide were bonded to a piezoelectric material. The results pointed to a comparable performance to that of the traditional quarter-wave layer matching. Opieliński *et al* [38] computationally analyzed the influence of changing material thicknesses (different from one-quarter wavelength) for the construction of a three-layer matching system in an ultrasonic airborne transducer. Comparing the results with that of three quarter-wave matching layers, they noted an enhancement in a transfer function relating the acoustic velocity to the input current. Most of the matching techniques require a layer or multi-layer of glue (or epoxy) for bonding purposes; hence, the thickness of glue must be taken into consideration [39]. However, the majority of past investigations considered zero-thickness glue in their design which undermines the performance of the matching systems. As such, the quarter-wave layer techniques, e.g., using a single matching layer whose characteristic impedance is the geometric mean of that of the medium and the transducer material, which also limits the choice of material, could not be practically implemented. Callens *et al* [40] proposed using a two-layer matching technique in water by considering the glue as one of the matching layers. Once the specific glue is selected, the choice of material for the other layer is very broad. In this approach, the thickness of selected materials needed to match a piezoelectric transducer at a desired resonant frequency can be accurately determined using a transfer matrix [41–43], which does not necessarily correspond to that of the quarter-wavelength material layers.

Recent investigations on UPT systems signified the effects of employing matching layers to further enhance contactless transfer of power through the acoustic medium between the piezoelectric transmitter and receiver [2, 44]. Accordingly, few analytical and experimental proof-of-concept studies have been conducted employing quarter-wave layer matching structures [45–48] and the aforementioned two-layer matching technique [5, 6, 10, 49] to improve the power transmission for ultrasonic implanted transducers in biomedical applications. However, the limited existing literature lacks a comprehensive analysis that can guide efforts to determine proper matching configurations for the fabrication process, i.e., the selection of the most efficient material layers and more importantly the estimation of material thicknesses needed to match a transducer at any desired frequency operating in an acoustic medium of interest. In this effort, we investigate a broad range of materials, considering two classifications, namely metals, some ceramics and composites, and polymers (plastics) using the two-layer matching structure first presented by Callens *et al* [40] in which we take into account the glue thickness. A four-layer matching system including two layers of glue and two layers of different materials is also evaluated to compare the performances of the two- and four-layer matching structures. Additionally, we consider the frequency-dependent ultrasonic material losses [30, 50, 51] for the receiver's electrical power output calculations to establish a trade-off between the attenuation effects and implementing matching layers depending on the acoustic medium.

In the UPT modeling, we assumed a piston-like motion for the piezoelectric receiver disk, where only the thickness mode of the disk resonates. This assumption holds for disks with an aspect ratio (diameter-to-thickness ratio) greater than 20 or less than 0.1, approximately [52, 53]. In this manuscript, the expressions *finite aspect ratio and finite size* refer to the aspect ratio between 0.1 to 20. We confirm that the disk, given as the case study in this paper, has an aspect ratio of 2.4, which is not on the reported acceptable range. Hence, using the reduced-order one-dimensional analysis of the finite-size receiver may lead to some deviations in the amplitudes of the electrical power output, when comparing with experiments [54]. However, the studied frequency range

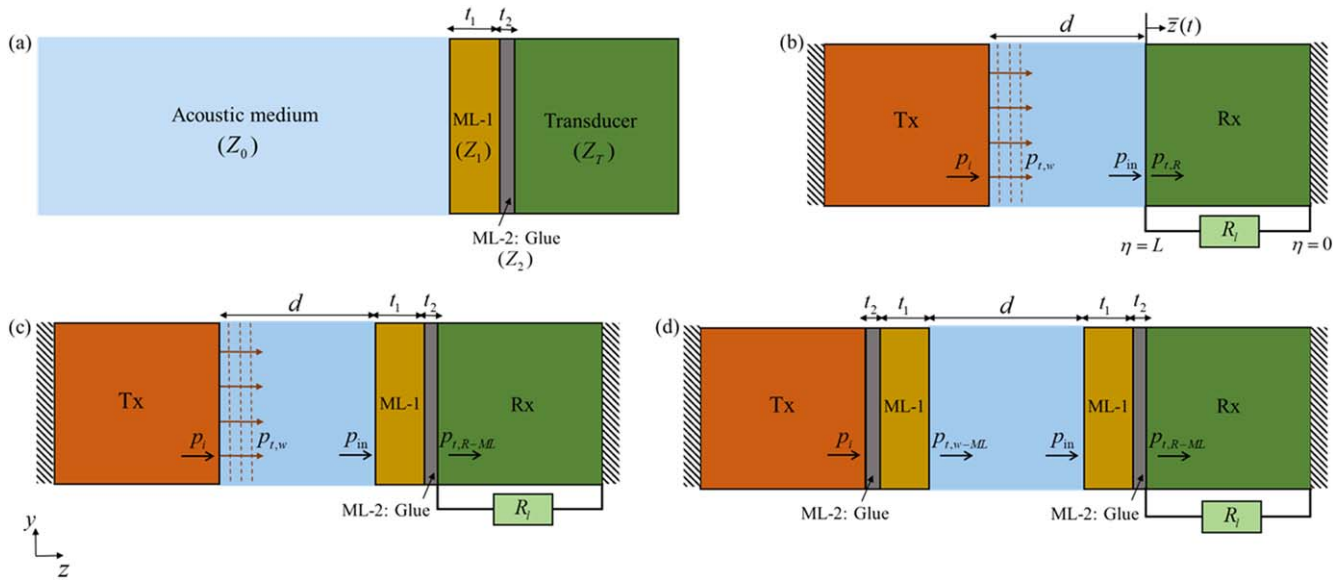

Figure 1. Schematic representation of various matching layer concepts. (a) An acoustically matched piezoelectric transducer using two matching layers: ML-1 and glue as ML-2. UPT-matching layer system consisting of Tx and Rx transducers with water as an acoustic medium in three case studies: (b) without matching layers, (c) matching Rx transducer only, and (d) matching both Tx and Rx transducers.

(300–700 kHz) was chosen in the domain, where the thickness mode of the disk is dominant; it is based on the information given by the manufacturer (APC International, Ltd), which was then validated by the measurement performed using an impedance analyzer (see figure A1). Additionally, the non-planar motion of the disk might also affect the scattered acoustic field through the radiation impedance and reflected acoustic field, which in turn changes the blocked (incident plus reflected) pressure. The study of non-planar motion effects, which are arising due to the finite aspect ratio of disks, can be implemented by a finite element-based approach, which is not the scope of this work. The focus of this work is qualitatively investigating the effects of acoustic impedance matching layers on the power transmission. Therefore, the given results, such as input acoustic pressures and electrical power outputs, are normalized.

Experiments are conducted to characterize the vibration response of the piezoelectric transmitter as well as the input excitation pressure to the receiver. In section 2, we present the theoretical model of acoustic impedance matching conditions and develop the model for the UPT-matching layer system, which couples the properties of the transmitter and receiver with the single and multiple matching layers. Results from experimental measurements and analytical models are discussed in section 3. A summary and conclusions are presented in section 4.

2. Analytical modeling: UPT-matching layer system

A schematic of an acoustically matched piezoelectric transducer to an acoustic medium with corresponding characteristic impedances Z_T and Z_0 is presented in figure 1(a). To quantify the power output enhancement by using matching layers, we consider three cases in a UPT system. The system includes a pair of similar PZT ultrasonic transducer disks in transmitter (Tx) and receiver (Rx) configurations operating in water. In case 1, shown in figure 1(b), no matching layer (ML) is added to the transducers. In case 2, shown in figure 1(c), matching layers are used for only the Rx transducer. In case 3, shown in figure 1(c), both Tx and Rx transducers include matching layers.

2.1. Acoustic matching technique

The transfer matrix for the nth material layer with characteristic acoustic impedance Z_n and thickness t_n, as shown in figure 1(a), considering a normally incident longitudinal plane wave through a multilayer system is written as [40, 41]

$$T_n = \begin{bmatrix} \cos(k_n t_n) & jZ_n \sin(k_n t_n) \\ \dfrac{j \sin(k_n t_n)}{Z_n} & \cos(k_n t_n) \end{bmatrix}, \tag{1}$$

where k_n is the wave number in the nth material. The transfer matrix represents the relation between pressure and normal particle velocity at the left and right boundary of the layer satisfying two boundary conditions, namely the *continuity of the pressure* and *continuity of the normal component of the velocity*. Because the thickness of the PZT transducer element is significantly larger than that of the matching layers, we assume a semi-infinite transmission line for the transducer material. The equivalent transfer matrix for the n-layer system is derived by defining

$$T^{eq} = T_1 T_2 \ldots T_n = \begin{bmatrix} T_{11}^{eq} & T_{12}^{eq} \\ T_{21}^{eq} & T_{22}^{eq} \end{bmatrix}. \tag{2}$$

Hence, the resultant equivalent acoustic impedance is written as

$$Z^{eq} = \frac{T_{11}^{eq} Z_T + T_{12}^{eq}}{T_{21}^{eq} Z_T + T_{22}^{eq}}. \tag{3}$$

Having determined the equivalent impedance, the power (intensity) reflection coefficient R_{I-ML} is derived by replacing the multilayer system to the right of the first layer, which according to figure 1(a) represents the acoustic medium, with an equivalent single boundary (two-layer) system to write (see equation (6.3.18) in [55])

$$R_{I-ML} = \left| \frac{Z^{eq} - Z_0}{Z^{eq} + Z_0} \right|^2. \tag{4}$$

The power (intensity) transmission coefficient T_{I-ML} is then defined as $T_{I-ML} = 1 - R_{I-ML}$.

Considering the two-layer matching system shown in figure 1(a), the power transmission coefficient is derived as

$$\begin{aligned} T_{I-ML} = {} & 8Z_0 Z_1^2 Z_2^2 Z_T / \{4Z_0 Z_1^2 Z_2^2 Z_T + 2(Z_0^2 Z_1^2 Z_2^2 \\ & + Z_1^2 Z_2^2 Z_T^2) \times \cos^2(k_1 t_1)\cos^2(k_2 t_2) \\ & + 2(Z_1^4 Z_2^2 + Z_0^2 Z_2^2 Z_T^2)\sin^2(k_1 t_1) \\ & \times \cos^2(k_2 t_2) + (Z_1^3 Z_2^3 + Z_0^2 Z_1 Z_2 Z_T^2 \\ & - Z_0^2 Z_1 Z_2^3 - Z_1^3 Z_2 Z_T^2) \times \sin(2k_1 t_1) \\ & \times \sin(2k_2 t_2) + 2(Z_0^2 Z_2^4 + Z_1^4 Z_T^2) \\ & \times \sin^2(k_1 t_1)\sin^2(k_2 t_2) + 2(Z_1^2 Z_2^4 \\ & + Z_0^2 Z_1^2 Z_T^2)\cos^2(k_1 t_1)\sin^2(k_2 t_2)\}. \end{aligned} \tag{5}$$

Perfect matching is achieved when the equivalent impedance is equal to the impedance of the acoustic medium in which there is complete transmission. Therefore, the power reflection coefficient becomes zero ($T_{I-ML} = 1$, $R_{I-ML} = 0$). Setting equation (3) equal to Z_0 and separating the real and imaginary parts, one obtains two expressions as follows:

$$\frac{T_{11}^{eq} Z_T}{T_{22}^{eq}} = Z_0, \tag{6}$$

and

$$\frac{T_{12}^{eq}}{T_{21}^{eq} Z_T} = Z_0, \tag{7}$$

in which equations (6) and (7) can be written as

$$A = \frac{Z_1 \tan(k_1 t_1)\tan(k_2 t_2) - Z_2}{Z_2 \tan(k_1 t_1)\tan(k_2 t_2) - Z_1}, \tag{8}$$

and

$$B = \frac{Z_1 \tan(k_1 t_1) + Z_2 \tan(k_2 t_2)}{Z_1 \tan(k_2 t_2) + Z_2 \tan(k_1 t_1)}, \tag{9}$$

where $A = \frac{Z_0 Z_2}{Z_1 Z_T}$ and $B = \frac{Z_0 Z_T}{Z_1 Z_2}$.

Likewise, the series of corresponding equations in a four-layer matching system containing two layers of glue with identical thickness t_2 ($t_2 = t_4$) and characteristic impedance Z_2, and two layers of different materials with thicknesses t_1 and t_3, and impedances Z_1 and Z_3, are obtained as

$$\begin{aligned} A = {} & \{2Z_1 Z_2 Z_3 \tan(k_1 t_1)\tan(k_2 t_2) + Z_2^2 Z_3 \tan^2(k_2 t_2) \\ & + Z_1 Z_2^2 \tan(k_1 t_1)\tan(k_3 t_3) + Z_2^3 \tan(k_2 t_2)\tan(k_3 t_3) \\ & + Z_2 Z_3^2 \tan(k_2 t_2)\tan(k_3 t_3) - Z_1 Z_3^2 \tan(k_1 t_1)\tan^2(k_2 t_2) \\ & \times \tan(k_3 t_3) - Z_2^2 Z_3\} / \{2Z_2{}^2 Z_3 \tan(k_1 t_1)\tan(k_2 t_2) \\ & + Z_1 Z_2 Z_3 \tan^2(k_2 t_2) + Z_2 Z_3^2 \tan(k_1 t_1)\tan(k_3 t_3) \\ & + Z_1 Z_2^2 \tan(k_2 t_2)\tan(k_3 t_3) + Z_1 Z_3^2 \tan(k_2 t_2)\tan(k_3 t_3) \\ & - Z_2^3 \tan(k_1 t_1)\tan^2(k_2 t_2)\tan(k_3 t_3) - Z_1 Z_2 Z_3\}, \end{aligned} \tag{10}$$

and

$$\begin{aligned} B = {} & \{Z_1 Z_2 Z_3 \tan(k_1 t_1) + 2Z_2^2 Z_3 \tan(k_2 t_2) - Z_1 Z_2 Z_3 \\ & \times \tan(k_1 t_1)\tan^2(k_2 t_2) + Z_2 Z_3^2 \tan(k_3 t_3) - Z_1 Z_2^2 \\ & \times \tan(k_1 t_1)\tan(k_2 t_2)\tan(k_3 t_3) - Z_1 Z_3^2 \tan(k_1 t_1) \\ & \times \tan(k_2 t_2)\tan(k_3 t_3) - Z_2^3 \tan^2(k_2 t_2)\tan(k_3 t_3)\} / \\ & \{Z_2{}^2 Z_3 \tan(k_1 t_1) + 2Z_1 Z_2 Z_3 \tan(k_2 t_2) \\ & - Z_2{}^2 Z_3 \tan(k_1 t_1)\tan^2(k_2 t_2) \\ & + Z_1 Z_2^2 \tan(k_3 t_3) - Z_2^3 \tan(k_1 t_1)\tan(k_2 t_2)\tan(k_3 t_3) \\ & - Z_2 Z_3^2 \tan(k_1 t_1)\tan(k_2 t_2)\tan(k_3 t_3) \\ & - Z_1 Z_3^2 \tan^2(k_2 t_2)\tan(k_3 t_3)\}. \end{aligned} \tag{11}$$

Using equations (8)–(11), we determine the thicknesses of glue and other material layers to acoustically match the transducers to the medium at a specific operating resonant frequency. The acoustic properties of the materials such as characteristic impedance and sound speed are known [26, 56, 57]. We compare the power transmission results with the ideal or theoretical quarter-wavelength layer system which uses a single layer whose characteristic impedance is the geometric mean of that of the medium and the transducer material ($Z_{\text{single-layer}} = \sqrt{Z_0 Z_T}$). Inevitably, the matching technique needs the glue layer(s) for bonding purposes and the choice of material whose impedance exactly equals $\sqrt{Z_0 Z_T}$ is limited. Hence, ideal matching could not be implemented in practice.

2.2. Closed-form voltage response of a piezoelectric receiver at steady state

The receiver disk treated as a fixed (clamped)-free [58] PZT cylinder operating in the 33-mode of piezoelectricity with fundamental resonant frequency in the range of 420–580 kHz (see figure A1 in appendix A). For the fluid-loaded and electrically-loaded fixed-free piezoelectric receiver disk excited by an acoustic wave (see figure 1(b)), the coupled partial differential equations for longitudinal vibration of the receiver and the AC electrical circuit equation are written as [1, 2]

$$-EA\frac{\partial^2 w(\eta,t)}{\partial \eta^2} - c_\gamma \frac{\partial^3 w(\eta,t)}{\partial \eta^2 \partial t} + c_\mu \frac{\partial w(\eta,t)}{\partial t} + R_r[\delta(\eta - L)]\frac{\partial w(\eta,t)}{\partial t} + m\frac{\partial^2 w(\eta,t)}{\partial t^2} - \kappa v(t)[\delta(\eta - L)] = f(t)[\delta(\eta - L)], \tag{12}$$

$$C_p \frac{dv(t)}{dt} + \frac{v(t)}{R_l} + \int_0^L \kappa \frac{\partial^2 w(\eta,t)}{\partial t \partial \eta} d\eta = 0, \tag{13}$$

where $w(\eta, t)$ is the displacement response of the disk at the axial position η and time t, $v(t)$ is the voltage output across the electrical load, E is the Young's modulus at constant electric field, $A = \pi a^2$ is the cross-sectional area, where a is the radius of the disk; m is the mass per unit length, c_γ is the stiffness-proportional damping coefficient, c_μ is the mass-proportional damping coefficient, κ is the electromechanical coupling term in physical coordinates, and $\delta(\eta - L)$ is the Dirac delta function. The parameters C_p and R_l, respectively, represent the internal capacitance of the piezoelectric receiver and the external load resistance. The excitation force due to the incident acoustic pressure $f(t) = p_{t,R}(t)A$ or $f(t) = p_{t,R-ML}(t)A$ is evaluated at the free-end surface ($\eta = L$) of the receiver. The forces are expressed in terms of transmitted acoustic waves captured by the PZT receiver (see figures 1(b)–(d)). Moreover, the dissipative term R_r in equation (12) is the resistive component of the fluid radiation impedance, which is given by equation (56) in [59] in terms of the normalized radiation resistance for an unbaffled circular transducer disk. The excitation of the receiver is such that the linear piezoelectricity is assumed and the elastic coupling and dissipative nonlinearities are not prominent.

The linear displacement at the free end of the piezoelectric receiver disk ($\bar{z}(t)$ in figure 1(b), where $\bar{z}(t) = w(L, t)$) due to harmonic excitation at or around the fundamental longitudinal axial vibration mode is obtained by modal analysis of the distributed-parameter electromechanical system for the fundamental mode of vibration. The longitudinal tip displacement of the piezoelectric receiver disk at time t is then written as

$$\bar{z}(t) = w(\eta, t)|_{\eta=L} = \varphi(L)\chi(t), \tag{14}$$

where $\varphi(L)$ and $\chi(t)$ are, respectively, the mass-normalized eigenfunction (mode shape) evaluated at $\eta = L$ and the generalized modal coordinate (temporal amplitude) for the longitudinal vibration mode of the fixed-free uniform disk. The mass normalized elastic-mode eigenfunction calculated from the corresponding undamped and electromechanically uncoupled (short-circuit) free vibration, is obtained as

$$\varphi(\eta) = \frac{\sin(\alpha\eta/L)}{\sqrt{\frac{mL}{2}\left(1 - \frac{\sin(2\alpha)}{2\alpha}\right) + m_r \sin^2(\alpha)}}, \tag{15}$$

where the eigenvalue, α, of the fundamental mode is the first non-zero root of the transcendental characteristic equation $(m_r/mL)\alpha \sin\alpha - \cos\alpha = 0$, where $m_r = X_r/\omega$ is the radiation mass, i.e., added mass, due to reactive component of the fluid radiation impedance which is given in equation (57) of [59] in terms of the normalized radiation reactance for the unbaffled disk, and ω is the excitation frequency. The radiation resistance (R_r) represents the actual power radiated by the vibrating surface to the fluid medium, whereas the radiation reactance (X_r) accounts for the stored energy of vibration near the surface which decreases the resonant frequency. Figure B1 in appendix B shows the normalized acoustic radiation resistance and reactance for unbaffled and baffled circular pistons (see equation (10.52) in [60]) as would be required in different applications.

The electromechanically coupled equations of forced vibrations and current balance for the fundamental vibration mode in the lumped-parameter form when reduced from the distributed-parameter solution are expressed as

$$\ddot{\bar{z}}(t)[1 - m_r\varphi^2(L)] + \dot{\bar{z}}(t)\left\{2\zeta\omega_r - c_\gamma\left[\varphi(\eta)\frac{d\varphi(\eta)}{d\eta}\right]_{\eta=L} + R_r\varphi^2(L)\right\} + \bar{z}(t)\left\{\omega_r^2 - \left[\varphi(\eta)EA\frac{d\varphi(\eta)}{d\eta}\right]_{\eta=L}\right\} - \kappa v(t)\varphi^2(L) = f(t)\varphi^2(L), \tag{16}$$

$$C_p\dot{v}(t) + v(t)/R_l + \kappa\dot{\bar{z}}(t) = 0, \tag{17}$$

where the over-dot represents differentiation with respect to time and ζ is the damping ratio defined by the mechanical quality factor Q ($\zeta = 1/2Q$) [61]. We shall note here that scattering effects and nonlinearity are assumed to be negligible for the receiver dimensions and considering low excitation amplitudes.

The steady-state electromechanical harmonic response is of the form $\bar{z}(t) = |\bar{z}|\, e^{j\omega t}$ and $v(t) = |v|\, e^{j\omega t}$ based on the linear system assumption, where j is the unit imaginary number. Here, $|\bar{z}|$ and $|v|$ denote amplitudes of the axial displacement and voltage output, respectively. Applying a damped boundary condition at $\eta = L$ in the modal coordinate, $[EA(d\varphi(\eta)/d\eta)\chi(t) + c_\gamma(d\varphi(\eta)/d\eta)\dot{\chi}(t) - \omega^2 m_r\varphi(\eta)\chi(t)]_{\eta=L} = 0$, and considering the harmonic vibration responses, the fundamental-mode output voltage amplitude frequency response function (FRF) is derived as

$$|v| = \left| \frac{-j\omega\kappa \times \left\{\begin{matrix}|p_{t,R}| \text{ or} \\ |p_{t,R-ML}|\end{matrix}\right\} \times A\varphi^2(L)}{(j\omega C_p + 1/R_l)\{\omega_n^2 - \omega^2 + j\omega[2\zeta\omega_n + R_r\varphi^2(L)]\} + j\omega\kappa^2\varphi^2(L)} \right|, \tag{18}$$

where ω_n is the fundamental resonant frequency. Consequently, the electrical power output FRF of the piezoelectric receiver disk (Π) is calculated using the equation $\Pi = v^2/R_l$.

2.3. Implementing the acoustic matching technique in UPT and including ultrasonic material losses

To compare the receiver's power output, we investigate the three case studies shown in figures 1(b)–(d). The amplitude of the transmitted pressure wave $p_{t,w}$ generated by the unmatched transmitter shown in figures 1(b) and (c) is calculated using the power transmission coefficient [55] as follows:

$$T_I = \left(\frac{Z_T}{Z_0}\right)\left(\frac{p_{t,w}}{p_i}\right)^2 = \frac{4Z_0Z_T}{(Z_0+Z_T)^2}. \tag{19}$$

On the other hand, the amplitude of the transmitted pressure wave $p_{t,w-ML}$ generated by the acoustically matched transmitter shown in figure 1(d) is calculated using the derived power transmission coefficient T_{I-ML} when implementing matching layers; $T_{I-ML} = (Z_T/Z_0)(p_{t,w-ML}/p_i)^2$. To find the incident acoustic pressure field, p_i, we measured the pressure distribution fairly close to the transmitter, as presented in section 3.3. The experimentally measured pressure field is then numerically back-propagated to the transmitter face to reconstruct the acoustic source field [62, 63] using the Near-field Acoustic Holography (NAH) method [64–66] via the Angular Spectrum Approach (ASA), which is explained in detail by the authors in [12]. Similarly, on the receiver side, the transmitted pressure waves $p_{t,R}$ (figure 1(b)) or $p_{t,R-ML}$ (figures 1(c) and (d)) are computed, respectively, using the expressions $T_I = (Z_0/Z_T)(p_{t,R}/p_{\text{in}})^2$ and $T_{I-ML} = (Z_0/Z_T)(p_{t,R-ML}/p_{\text{in}})^2$. Likewise, the input pressure p_{in} is calculated numerically via the ASA by forward-propagating the transmitted pressure field $p_{t,w}$ or $p_{t,w-ML}$. Finally, the power output for the PZT receiver is calculated using equation (18) and $\Pi = v^2/R_l$.

Additionally, the amplitude of the ultrasonic wave is attenuated as it passes through the medium and material layers. To account for losses of acoustic energy, a lossy Helmholtz equation $\nabla^2 p + \boldsymbol{k}^2 p = 0$ with the complex wave number $\boldsymbol{k} = k - j\beta = \omega/\boldsymbol{c}$, is developed [55], where β is a frequency-dependent attenuation coefficient, $\boldsymbol{c}$ is the complex stiffened wave speed (complex speed of sound), and the harmonic plane wave pressure p is expressed as

$$p = |p|\, e^{-\beta z} e^{j(\omega t - kz)}. \tag{20}$$

The electrical power output for the UPT system is then reduced by a power attenuation factor μ defined as [47, 67]

$$\mu = e^{-2\sum_i \beta_i z_i}, \tag{21}$$

where z_i represents the thickness of matching layers, as well as the distance between the transmitter and receiver. It should be noted that the amplitudes of the voltage and electrical power output are, respectively, proportional to the first and second power of the amplitude of the transmitted pressure waves captured by the receiver. As a result, the acoustic power enhancement by implementing matching layers in the UPT system considering the acoustic attenuation is determined.

It should be emphasized that in the UPT analysis, we consider a lossy transducer using the damping ratio of the PZT transducer through the mechanical quality factor, $\zeta = 1/2Q$, in equation (16). However, we neglect a dielectric loss factor which can be easily included considering the complex capacitance for the piezoelectric material [68, 69] ($\boldsymbol{C_p} = C_p(1 - j\delta_{tn})$, where δ_{tn} represents the dielectric loss factor, which usually referred to the loss tangent). Note that the loss tangent of the PZT disk used in this study is around 2%, which only changes the capacitance by 0.02%. Moreover, we take into account the attenuation coefficient β for the medium and matching layers for the decaying plane (pressure) wave in equation (20) and later in computing the electrical power output. Note that we neglect the attenuation in specific acoustic impedance calculations. Finally, the effect of fluid damping is included through the dissipative term R_r in equation (12).

3. Experiments and theoretical results

3.1. Frequency response of the transmitter in water: measured surface velocity

The experiments were conducted on a cylindrical 33-mode PZT disk (APC850-Navy II from APC International, Ltd [70]) having a diameter of 9.5 mm and a thickness of 3.9 mm. The density of the disk is 7600 kg m^{-3} [71] and the speed of sound in the PZT material is 4780 m s^{-1} which results in $Z_T = 36.3$ MRayl. The disk's surface velocity was measured using a laser Doppler vibrometer (LDV, including Polytec OFV-505 sensor head and Polytec OFV-5000 controller) and acquired using a 1-GS/s digital oscilloscope (Tektronix TBS 2000 series, model TBS2104) with 512 averages. During underwater actuation experiments, the disk was excited by an average input voltage of 44 V peak-to-peak using a waveform generator (Keysight 33500B series) that was connected to an amplifier (E&I RF power amplifier, model A075). The disk was bonded to a thin brass plate using a thin layer of high-shear-strength epoxy (3M DP460 Scotch-Weld Epoxy Adhesive) and then the plate was mounted in a watertight box made of an acrylic sheet with the help of a neoprene rubber sheet as shown in figure 2(a) and similarly to the procedure explained in [72]. We used the box in order to electrically insulate the PZT transducer in water and to construct the air-backed transducer which reflects almost all power from the backside of the transducer toward the transmission line and enhances the power transfer. The box including the PZT disk was fully submerged in 615 mm × 318 mm × 325 mm tank of deionized water. The surface velocity FRF of the disk is presented in figure 2(b) indicating an underwater fundamental resonant frequency of 510 kHz, which is considered as the desired frequency for acoustically matching the transmitter and receiver transducers using matching layers. Noticeably, the observed both radial and thickness vibration modes occur due to the finite aspect ratio of the disk, which makes the assumption of the piston-like motion, where the disk vibrates only in the thickness direction, not quite accurate but acceptable in the frequency range of interest.

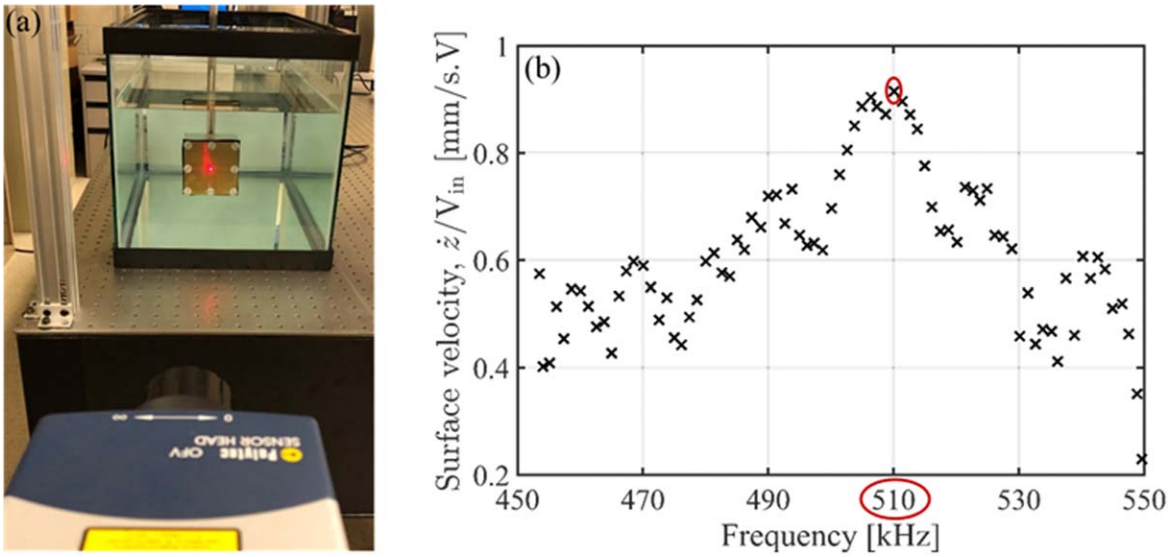

Figure 2. (a) Underwater actuation experimental setup and (b) corresponding measured surface velocity of the PZT transducer versus excitation frequency, which shows a transducer's underwater resonant frequency of 510 kHz.

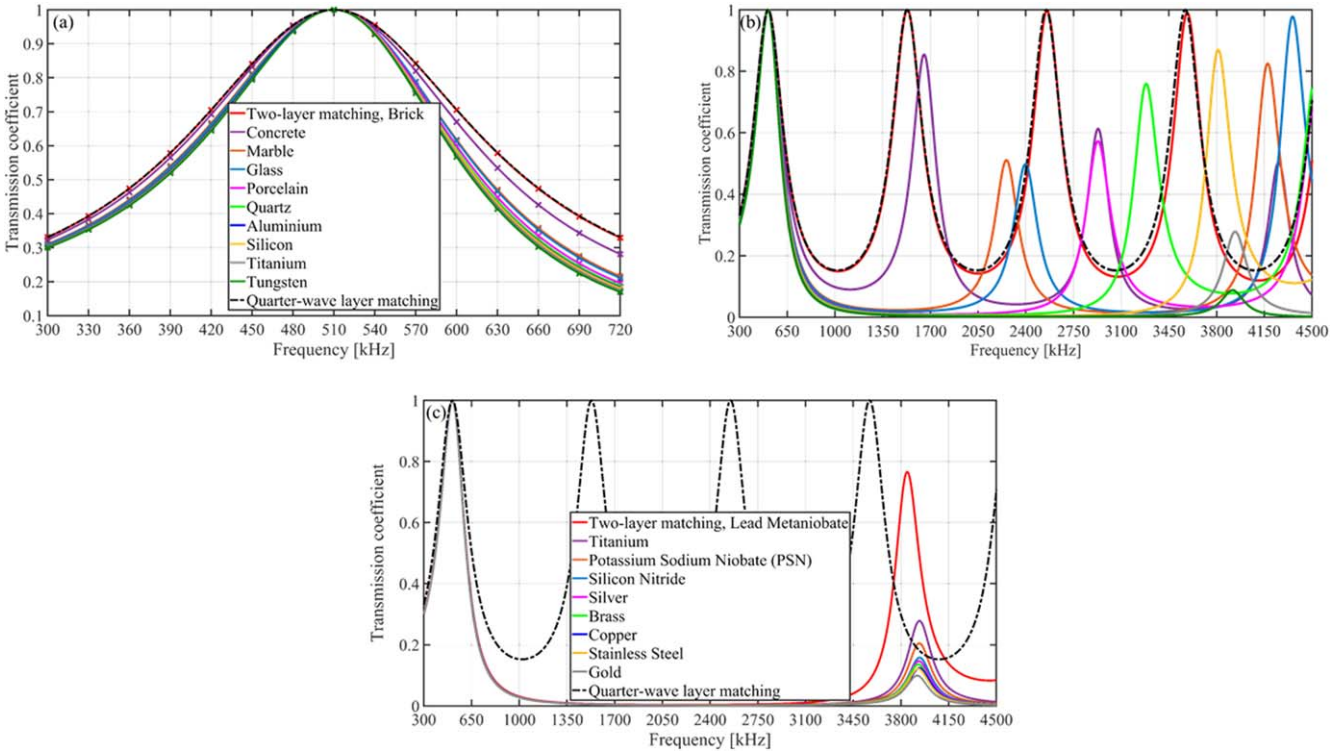

Figure 3. Power transmission coefficient of the matched PZT transducer implementing the two-layer matching structure with different materials (metals, ceramics, and composites) as ML-l and glue A as ML-2, compared with the ideal matching system: (a) frequency range from 300–720 kHz, and (b) 300 kHz–4.5 MHz, and (c) investigations of more material choices. The legend in (b) is set the same as that of (a). The cross markers in (a) represent the driving frequencies for which we have experimentally measured the pressure fields generated by the transmitter transducer, later shown in figure 9.

3.2. Materials selection in the two-layer acoustic matching technique: Thicknesses determination

For the two-layer structure implemented for matching the PZT disks ($Z_T/Z_0 = 24.2$), we investigated two main groups of materials: (1) several types of metals as well as some ceramics and composites for the first matching layer (ML-1) and an Araldite glue [56] with specific acoustic impedance of 3.04 MRayl and a longitudinal sound speed of 2620 m s^{-1} (glue A) as the second layer (ML-2); and (2) polymers or plastics as ML-1 and an Araldite glue [56] with specific acoustic impedance of 12.81 MRayl and a longitudinal sound speed of 1520 m s^{-1} (glue B) as ML-2.

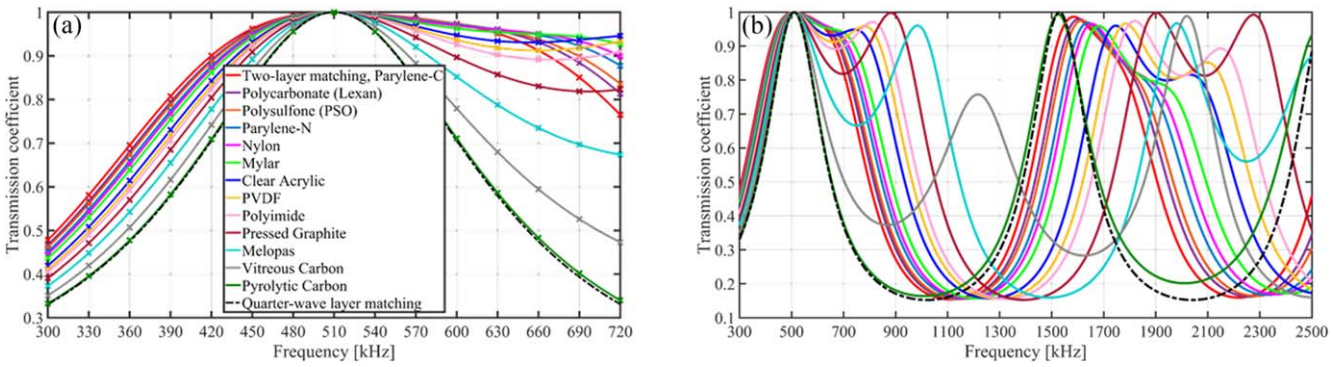

Figure 4. Power transmission coefficient of the matched PZT transducer implementing the two-layer matching structure with different polymers (or plastics) as ML-l and glue B as ML-2, compared with the ideal matching system: (a) frequency range from 300–720 kHz, and (b) 300 kHz–4.5 MHz. The legend in (b) is set the same as that of (a). The cross markers in (a) represent the driving frequencies for which we have experimentally measured the pressure fields generated by the transmitter transducer, later shown in figure 9.

Figure 3(a) shows the acoustic power transmission coefficient in the first matching type using materials such as aluminum, titanium, glass, and porcelain for ML-1 and glue A for ML-2 compared with the transmission from the theoretical or ideal single (quarter-wave layer) matching. Apparently, the full width at half maximum (FWHM) of the two-layer system is comparable to that of ideal matching, e.g., using brick as ML-1, the system exhibits almost the same transmission performance as the quarter-wave layer matching. Moreover, the selection of different materials to acquire a relatively good transmission for the frequency range shown in figure 3(a) leads to comparable performances. However, as the frequency range is increased, more peaks appear in which selection of different materials for ML-1 leads to dissimilar performances as shown in figure 3(b). To illustrate, choosing brick, represented by the red curve in figure 3(b), as ML-1, one obtains several peaks of transmitted acoustic energy for the transducer, whereas choosing glass, represented by the blue curve in figure 3(b), as ML-1, results in two peaks of higher transmission other than the fundamental frequency, where good transmission is obtained only at a frequency around 4.4 MHz. It should be emphasized that we considered the performance of matching by analyzing only the acoustic power transmission coefficient; however, later for analyzing the electrical power output performance, the acoustic attenuation must also be taken into consideration as detailed in section 3.3. Figure 3(c) demonstrates the power transmission coefficient of the matched transducer analyzing other material choices for ML-1 such as commonly used metals like silver, copper, and stainless steel as well as some other ceramics such as lead metaniobate. It is determined that these materials show the same performance in acoustic matching as that of titanium up to about 3 MHz. However, the materials' effectiveness starts to diverge near 3.5 MHz.

The second matching type is performed by employing polymers as ML-1 and glue B as ML-2. The power transmission coefficient for the matched transducer is presented in figure 4(a). Clearly, the two-layer matching technique in this type leads to a wider frequency bandwidth compared to the ideal matching and to the first matching type depicted in figure 3. Evaluating the acoustic transmission over wider frequency range, the observed trends of transmission as shown in figure 4(b) are different than those of figure 3(b) in which the quality and intensity of most of the peaks, generated from the choice of polymers, are more noticeable. Furthermore, it should be noted that at the fundamental frequency of 510 kHz, all material choices lead to the maximum power transmission coefficient of unity as shown in figures 3 and 4, which shows the reliability of the transfer matrix method in determining the accurate thicknesses for the two layers to match the PZT transducer at the desired resonant frequency operating in water. It is also worthwhile to remark that some of the selected materials in this study are recognized to be biocompatible such as glass [10], titanium [48, 73], pyrolytic carbon [5, 73], and parylene [44].

The results of the acoustic matching techniques presented above were verified in two ways. Firstly, we verified the claim that implementing these techniques enhances the acoustic power transmission at any desired resonant frequency and also improves the transduction bandwidth leading to a wider frequency bandwidth. Figure 5(a) shows three scenarios for constructing a PZT transducer, namely (i) implementing the two-layer matching technique with layers of glass and glue A for the transducer, (ii) implementing a single classical quarter-wave layer matching technique, and (iii) using the transducer without matching layers. The power transmission coefficient for the latter scenario is calculated assuming four material layers of water, acrylic for fixing the backside of the transducer disk to an acrylic holder with a thickness of 3 mm (see figure 8 in [12]), PZT with a thickness of 3.9 mm, and again water (front side of the disk). Figure 5(a) clearly indicates the enhancements of the power transmission at the desired frequency of 510 kHz for the acoustically matched transducers compared to that of the unmatched transducer. The transducer without matching layers has the highest power transmission coefficient value of 0.87 at 598 kHz instead of the unity value at the desired frequency. Moreover, a noticeable bandwidth improvement is observed in the matched transducers. The relative bandwidth at -3 dB (half-power bandwidth) at the center frequency of 598 kHz for the transducer without matching layers is 7.9%, compared to that of 47.6% and 55.7% at the center frequency of 510 kHz for the transducers

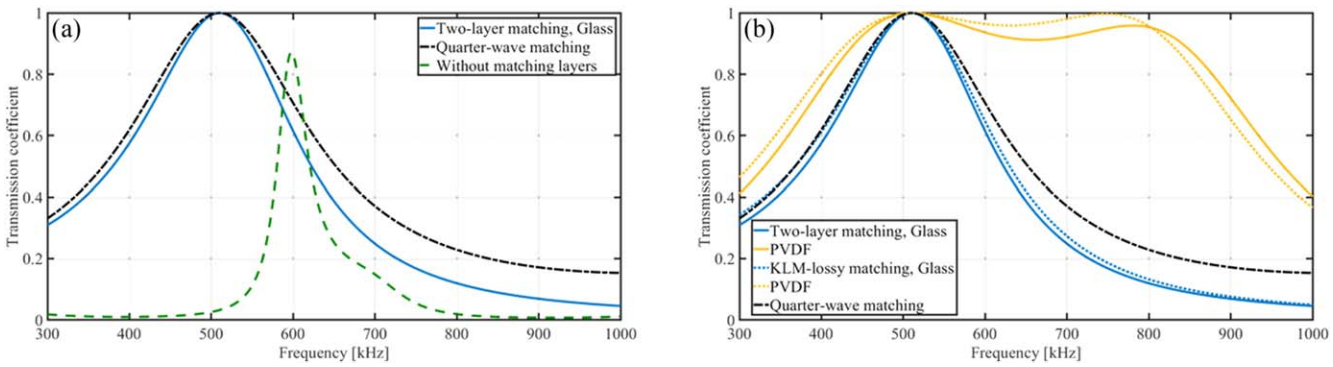

Figure 5. Comparing the power transmission coefficient of the acoustically matched PZT transducers using the two-layer and quarter-wave matching techniques (a) to that of the unmatched transducer, and (b) to that of the matched transducers using the KLM-lossy matching technique (dotted lines) adopted from [10, 68]. Glue A and B are used for bonding the layer of glass and PVDF, respectively.

having the two-layer and quarter-wave matching, respectively.

Secondly, we compared the two-layer and quarter-wave matching techniques, which we have assumed the semi-infinite thickness for the PZT transducer, to the KLM model [10, 74] in which the effects of backing layer, electrical load, and thickness of the PZT material are also taken into account for the power reflection coefficient calculation. Moreover, we consider losses in the KLM model in which the losses are associated with the dielectric loss factor [68, 69, 75] through the loss tangent of 2%, as well as the ultrasonic attenuation which results in the complex stiffened wave speed in the PZT material [68, 69, 75, 76]. Figure 5(b) shows three scenarios for constructing a PZT transducer, namely (i) implementing the two-layer matching technique with layers of glass and glue A, as well as layers of PVDF and glue B for the transducer, (ii) using the same materials for ML-1 and ML-2 with the aforementioned KLM-lossy matching technique, and (iii) using a single classical quarter-wave layer matching. The power transmission coefficient for the matched transducer implementing the KLM-lossy model is calculated as explained in section 2.1 with a modification in computing the PZT acoustic impedance, Z_{pzt}, by applying equations (3)–(14) in [10], as well as equations (1) and (4) in [68]. We also set the acoustic impedance of the backing layer, $Z_{backing}$ (see equation (11) in [10]), as that of acrylic material for fixing the backside of the transducer disk. Furthermore, in the KLM model, the electrical load resistance is set to 1.55 kΩ, which is the optimal electrical load at 510 kHz (see figure 9(d)) and no inductor is used. The relative bandwidth at −3 dB at the center frequency of 510 kHz for the transducer having the layers of PVDF and glue B using the two-layer matching technique is 124.2%; while for the transducer having the same material layers implementing the KLM-lossy model is 124.1%. For the transducer having the layers of glass and glue A, the relative bandwidth at −3 dB at the center frequency of 510 kHz using the KLM-lossy matching technique is 51.3% compared to that of 47.6% in the two-layer matching model as mentioned before. Hence, although the two-layer matching technique implemented in this paper neglects the effects of the backing layer, electrical load, thickness of the transducer, and dielectric loss factor on the acoustic reflection, it is in a very good agreement with that of the KLM-lossy matching technique that considers all the above effects.

Considering all material choices, we present in figure 6 a design platform that can be used to guide the development and design of proper two-layer matching configurations using selected glues A or B. Hence, once the specific glue is taken as ML-2, the material for ML-1 can be selected based on its characteristic acoustic impedance. The corresponding thicknesses for both layers, which are the key parameters in matching performance, can then be easily determined. Moreover, benefiting from the non-dimensional wave number kt in figure 6, we propose that similar design platforms could be obtained for acoustically matching transducers at any desired resonant frequency operating in an acoustic medium of interest, using any type of glue or epoxy. As a result, we can facilitate the construction of high-fidelity matched transducers to enhance acoustic power transmission. A comprehensive and detailed list of materials analyzed in this study for the two-layer matching system with their acoustic properties obtained from literature [26, 56, 57] is tabulated in appendix C as tables C1 and C2 to aid the readers in the design of acoustically matched transducers. The thicknesses of both ML-1 and ML-2 (glue A or B) calculated for matching the transducer at 510 kHz are also provided in the table.

3.3. Electrical power output enhancement in UPT implementing acoustically matched transducers

As noted in section 2, we investigate three UPT system cases comprising the piezoelectric transmitter (Tx) and receiver (Rx) disks with the same size as shown in figures 1(b)–(d) and are respectively referred to as (1) *without matching layers* case, (2) *only Rx* case, and (3) *Tx and Rx* case. The distance d between the transmitter and receiver is set to 60 mm and it is assumed that the Tx and Rx transducers are perfectly aligned and that the receiver has a fixed-free boundary condition. The electrical power output for the receiver excited by the incident acoustic wave from the transmitter is estimated using equation (18) and $\Pi = v^2/R_l$, considering the aforementioned three case studies to assess system enhancement using matching layers.

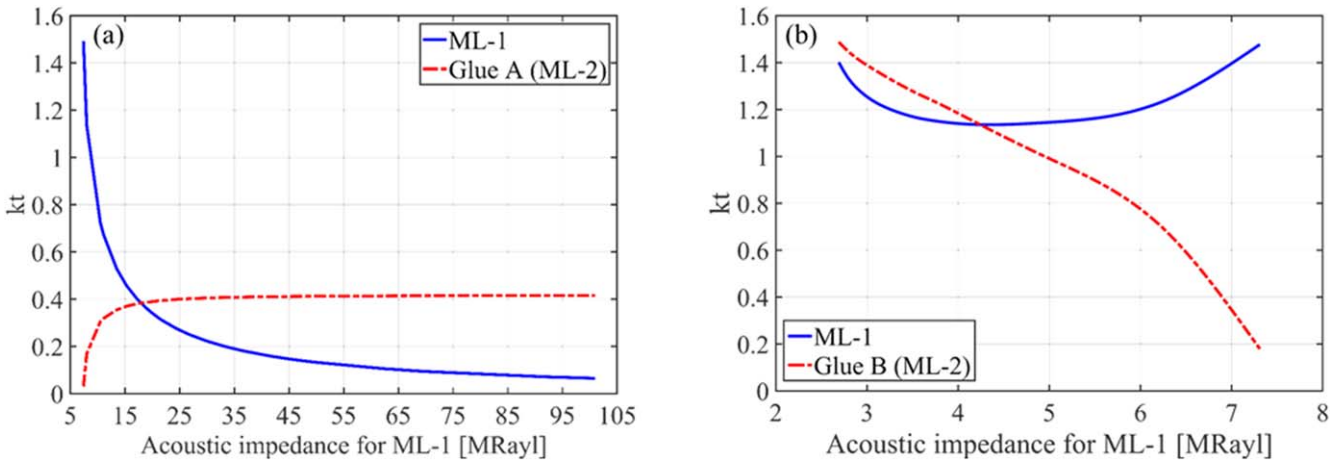

Figure 6. Design platform to find the proper two-layer matching configuration to select a material for ML-1 and determine thicknesses for both layers using (a) glue A and (b) glue B.

The experiments were performed to find the average input excitation force on the receiver disk due to the incident acoustic pressure from the transmitter. To calculate the input force, the transmitter output pressure field is reconstructed from the experimentally measured pressure field close to the source via the ASA (see section 2.3), which is then used to determine the average pressure on the plane, where the receiver is located, at 60 mm from the source, using the propagation function described in [12, 77]. We measured the sound pressure in a plane at the distance 30 mm using a calibrated 0.2 mm needle hydrophone (Precision Acoustics Ltd with the sensitivity 50.6 mV/MPa at 500 kHz) mounted on a manufactured 3D positioning system as depicted in figure 7. The hydrophone preamplifier was connected to a DC coupler with power supply (Precision Acoustics Ltd) referenced to the digital oscilloscope in which the hydrophone signal was acquired and a developed MATLAB script is used that scans the acoustic field in the 2D measurement plane. The disk was excited by the low average input voltage of 21 V peak-to-peak to ensure that the PZT disk maintains the same performance over the one-hour hydrophone scan. The deionized water tank was partially lined with acoustic absorber sheets (Aptflex F28, Precision Acoustics Ltd) to avoid reflections from the tank walls. The pressure measurements were conducted over a range of driving frequencies between 300 and 720 kHz with 30 kHz increments. The measurement at each position on a plane at 30 mm distance from the transmitter was averaged over three times. The aperture of the measurement plane was about 50% wider than the diameter of the disk. We set the spatial resolution of 0.2 mm, which is smaller than one-half wavelength in the medium, to avoid aliasing [63].

The procedure for calculating the average input acoustic pressure on the receiver is illustrated in figure 8, where pressure distributions at 510 kHz using one of the analyzed matching materials are presented. Figure 8(a) shows the back-propagated pressure on the boundary between the transmitter and water, and figures 8(b) and (c) present the input pressures on the receiver face considering two scenarios of using no impedance matching material and implementing layers of glass ($\beta_{\text{glass}} = 1.15$ Np m^{-1} measured at 2 MHz [78]) and glue A ($\beta_{\text{glue}} = 173$ Np m^{-1} measured at 4 MHz [79]) for the transmitter, respectively. The dashed circles in figure 8 represent the locations of the transmitter (orange circle) and receiver (green circles) disks. It is noted that the average input pressure on the receiver surface using the matched acoustic source is significantly increased, which shows 2.5 times higher value in comparison to that of using the unmatched transmitter (note that $T_I = 0.15$ from equation (19) and $p_{t,R} \propto \sqrt{T_I}$). This can also be concluded from a comparison of the values in figures 9(a) and (b).

Figures 9(b) and (c) present the average input pressure values due to acoustic excitation from the transmitter, by implementing the investigated matching materials, including, respectively, the first and second material types as illustrated in figures 3(a) and 4(a). In order to make a fair comparison between the unmatched and matched cases, the pressure values in figure 9(a), which are obtained for a UPT system with the unmatched acoustic source, are normalized by the maximum pressure existing for the first matching type shown in figure 9(b). The results clearly show the effectiveness of using the impedance matching technique. The maximum excitation pressure at 510 kHz is generated using glass, as the first matching type in figure 9(b), and vitreous carbon, as the second matching type in figure 9(c). The generated pressure for using glass is slightly higher, compared to that of vitreous carbon. The pressure attenuation factor $e^{-\beta z}$ for each matching structure is taken into account in figures 9(b) and (c) based on the attenuation coefficient of material layers and the calculated thicknesses for ML-1 and glue. The attenuation in water ($\beta_{\text{water}} = 0.023$ Np m^{-1} measured at 1 MHz [80]) is accounted for on the basis of the distance between the transmitter and receiver transducers. The observed values of the attenuation coefficient for the selected materials in this study are provided in appendix C as extracted from the literature. It should be noted that the values are roughly calculated for the frequency range of 300–720 kHz assuming a proportional increase of losses to the first power of frequency for the matching materials and to the second power of frequency for water. As depicted in figures 9(b) and (c), brick and PVDF possess the highest acoustical loss leading to the

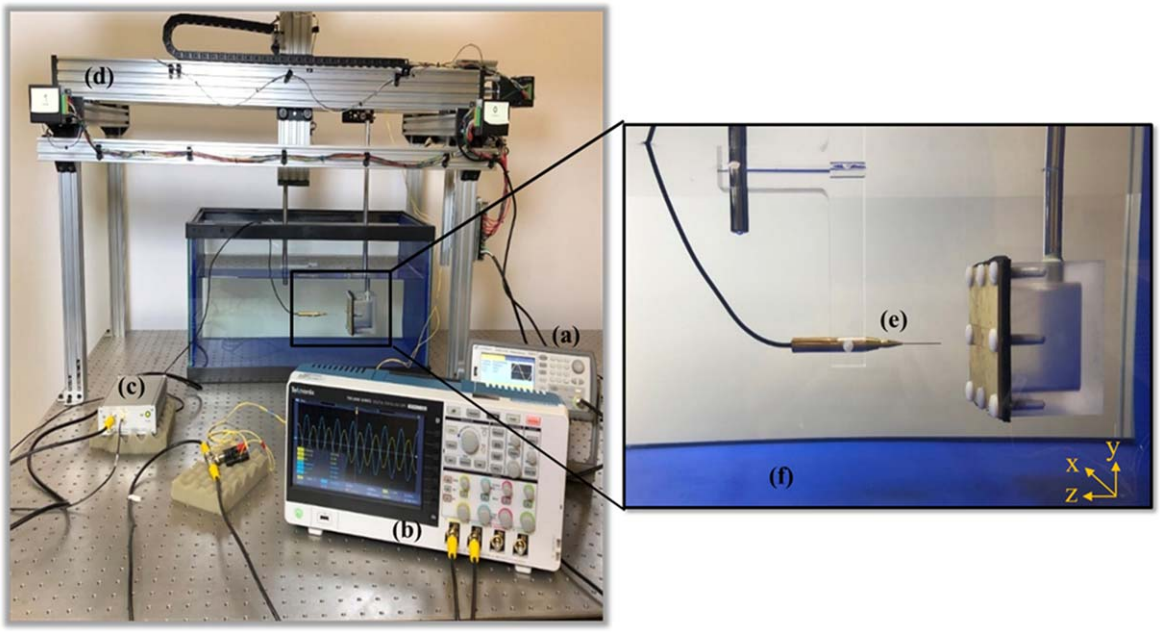

Figure 7. Experimental setup for measurement of pressure fields generated by the PZT transmitter disk enclosed in the watertight box: (a) waveform generator, (b) digital oscilloscope, (c) DC coupler with power supply, (d) positioning system, (e) needle hydrophone, and (f) acoustic absorber sheet).

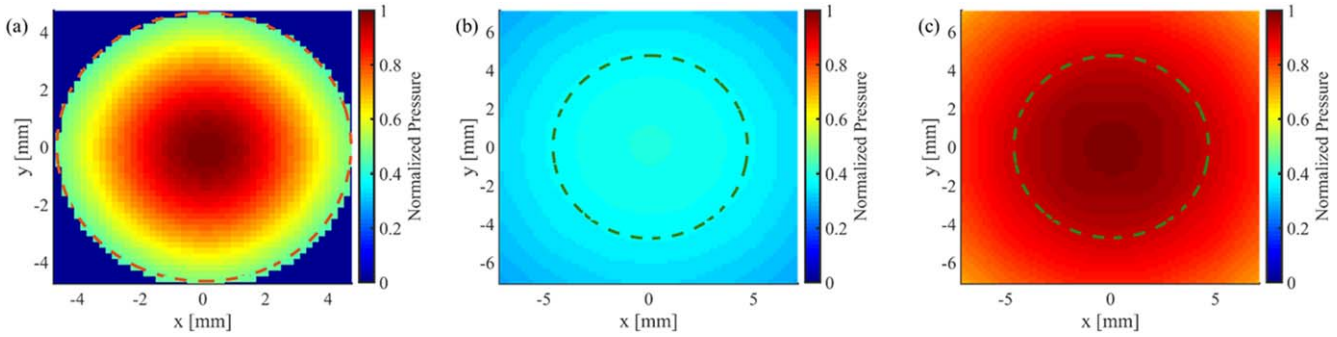

Figure 8. Acoustic pressure distributions at 510 kHz including (a) the back-propagated field at the boundary between the transmitter and water from experimentally measured pressure field, normalized by the maximum value in (a); the forward-propagated field in the plane, where the receiver is located at $d = 60$ mm in which the disk is excited by the incident acoustic wave from the acoustically (b) unmatched, and (c) matched transmitter using layers of glass and glue A. The pressures in (b) and (c) are normalized by the maximum value in (c).

lowest generation of the input acoustic pressure on the receiver using these materials for acoustically matching the transmitter.

Evidently, the attenuation plays a significant role in selecting the matching scheme in UPT as noted from the trend of the input pressure in figures 9(b) and (c), which is considerably different from that of the power transmission coefficient shown in figures 3(a) and 4(a). This is due to the fact that in calculating the power transmission coefficient, no attenuation is taken into account leading to the value of unity for all the selected materials at 510 kHz. Moreover, in figure 9(c), one can see that the pressure increases monotonically, even at frequencies greater than 510 kHz. This occurs only due to the higher values of measured pressure at the frequency range of 540–720 kHz while their corresponding power transmission coefficient values in figure 4(a) are less than unity. The input pressure using the quarter-wave matching structure shown in figures 9(b) and (c) is also calculated with a single layer of another type of Araldite epoxy (glue C) with the specific acoustic impedance of 7.45 MRayl [56], which is close to the geometric mean of water and the transducer PZT material impedances, considering the loss of 173 Np m^{-1} (measured at 4 MHz). Of interest is the realization that the maximum pressure is not necessarily achieved using ideal matching conditions. The electrical load resistance in equation (18) is set to that of the optimal load that gives the maximum electrical power output at each analyzed driving frequency. The power output normalized with the excitation force ($f(t) = p_{t,R}(t)A$ or $f(t) = p_{t,R-ML}(t)A$) squared is shown in figure 9(d) in which the optimal load at each frequency can be determined. Other parameters, namely electromechanical coupling, capacitance, and mechanical quality factor of the receiver are, respectively, set to $\kappa = 0.21$ C m^{-1}, $C_p = 180$ pF, and $Q = 70$, which were identified by measuring the electrical impedance of the receiver disk in air and fitting it to

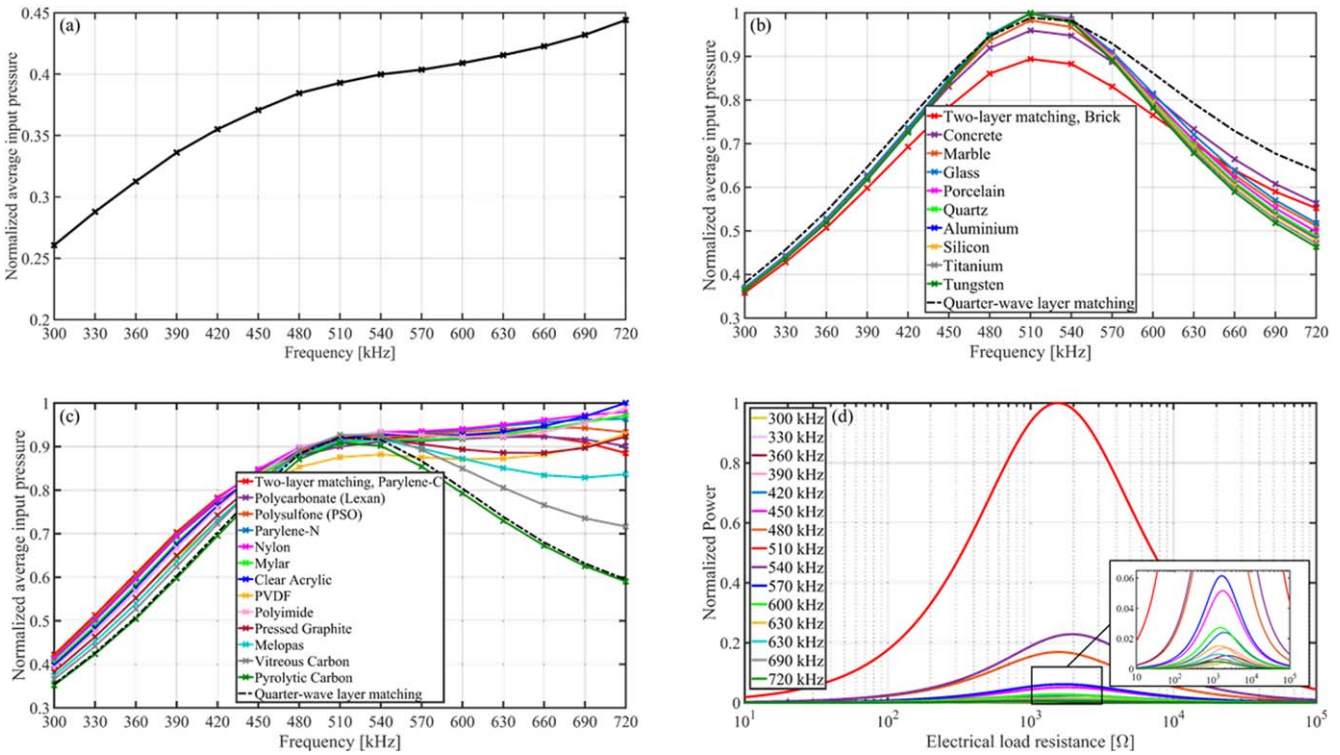

Figure 9. Calculated average input pressures on the surface of the receiver excited by (a) the unmatched transmitter. The average input pressures on the receiver excited by the matched transmitter (b) using the first matching type (with glue A), and (c) using the second matching type (with glue B). (d) Electrical power output (normalized with respect to the excitation force squared) versus electrical load resistance for each analyzed driving frequency, showing the optimal load in the range of 1.26–2.85 kΩ. The pressures in (a) are normalized by the maximum value in (b) and the pressures in (b) and (c) are normalized by the maximum value in each type. The results for the single quarter-wave matching system using glue C are also shown in (b) and (c). The power output values in (d) are normalized by the maximum value in (d).

the UPT analytical model in the frequency range of 420–580 kHz. Figure A1 in appendix A shows the measured electrical impedance of the unloaded disk in air using the HP4192A impedance analyzer in the frequency range of 100–700 kHz in which one can see both the radial and thickness vibrational modes of the finite-size receiver disk; in the range of 300–700 kHz, the thickness vibration mode of the disk is dominating.

Figure 10 shows the power output of the UPT system analyzed in the three scenarios as depicted in figures 1(b)–(d). Noticeably, the maximum power output of the system, at the resonant frequency of 510 kHz, improves when the transducers were acoustically matched with the medium. The results in figures 10(a) and (b) show a power gain enhancement of 8 dB comparing the maximum power values achieved using glass and vitreous carbon for *only Rx* case with that of *without matching layers* case, as well as comparing the maximum power value for *Tx and Rx* case with that of *only Rx* case. However, the improvements are reduced using other materials with higher attenuation to a maximum level of 36% using brick as shown in figure 10(a) and a maximum level of 20% using PVDF as shown in figure 10(b). The attenuation variations with frequency for the selected material layers and water in a broad ultrasound frequency range of 20 kHz–10 MHz is presented in figure D1 in appendix D. At higher frequencies, the ultrasonic material losses limit the level of power improvement, particularly in lossy media, i.e., the media with high attenuation coefficient, such as human tissue, which has excessively higher attenuation value than water [81]. In our investigation, PVDF has the highest levels of acoustic loss of 154.3 Np m^{-1} [82] (measured at 1 MHz) resulting in a power attenuation factor of $\mu = 0.76$ at 510 kHz and $\mu = 0.57$ at 10 MHz (see figure D1) for the *Tx and Rx* case results presented in figure 10(b), which appears that yet the matching technique overcomes the losses in water at high frequencies. However, considering human tissue, using matching layers most likely downgrades the power enhancement at high frequencies. We shall also note that as the frequency increases, the proportionally thinner matching layers are required to match the transducers, hence, only the power attenuation factor in the acoustic medium increases. Comparing the power output enhancement using two types of matching layers in figures 10(a) and (b), an increase of 3% is obtained using glass in comparison to vitreous carbon. However, some enhancements are seen at off-resonance frequencies, noticeably at higher frequencies, where polymers or plastics appear to be better material choices. Furthermore, the higher power improvement is attained comparing the two-layer structures with glass, porcelain, quartz (X-cut), silicon, aluminum, titanium, tungsten, vitreous carbon, and polyimide, to that of the ideal matching with the single layer of epoxy. In general, it is concluded that implementing acoustic impedance matching layers in UPT systems is of utmost importance for acquiring efficient electrical power output from the receivers/sensors; however, the material losses must be also taken into consideration to ensure that the trade-off between the matching technique and attenuation effects are reasonable.

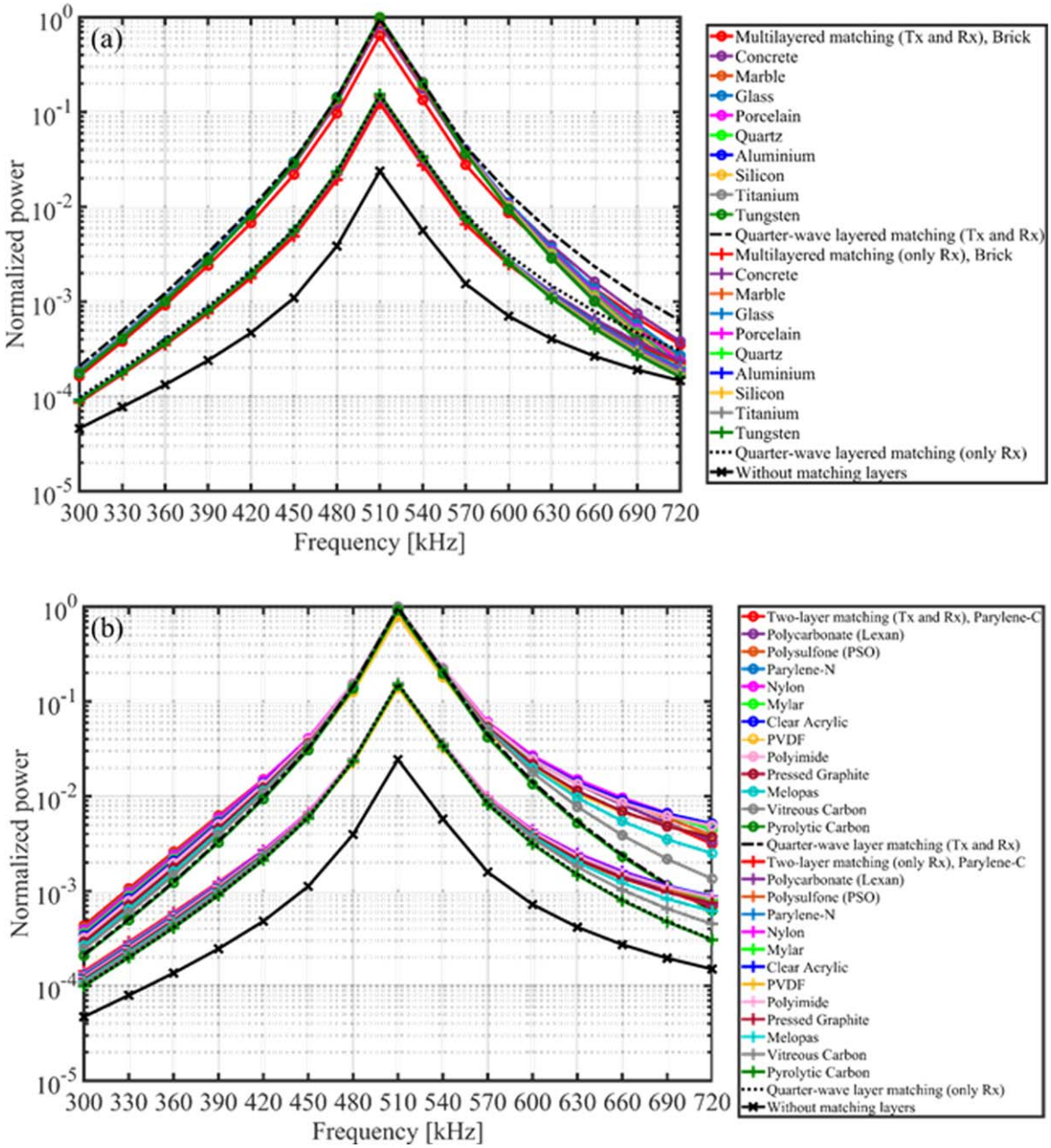

Figure 10. (a) Electrical power output for the piezoelectric receiver at $d = 60$ mm excited by the acoustic source, analyzed in three scenarios in the UPT system, namely *without matching layers* case depicted with a cross marker, *only Rx* case depicted with plus sign markers, and *Tx and Rx* case depicted with circle markers using (a) first matching type (with glue A), and (b) second matching type (with glue B). The power output values are normalized by the maximum value in each type. The results for the single quarter-wave matching system are also shown in (a) and (b), which dotted and dashed-dot lines, respectively, represent *only Rx* case and *Tx and Rx* case using glue C.

3.4. Implementing a four-layer acoustically matching technique in UPT

We also investigated four-layer matching systems containing two layers of glue A and two layers of different materials such as using a combination of glass and acrylic as shown in figure 11(a), and also a combination of polymer and metal layers as shown in figure 11(c), where a layer of polyethylene is selected in conjunction with a metal layer, namely titanium, silver, brass, copper, and steel. In figures 11(a) and (c), the thickness of glue layers are, respectively, set to 0.2 and 0.25 mm. Comparing the results of the acoustic power transmission coefficient with those of the two-layer system containing the same glue with a layer of glass and metals, it is concluded that adding matching materials leads to a relatively wider frequency bandwidth in which the FWHM of the four-layer configuration is very close to the ideal matching or slightly enhanced. However, the maximum transmission is achieved for both two and four-layer structures and only some improvements at off-resonance frequencies are observed. Analyzing the acoustic transmission of the matched transducer over the wider frequency range shown in figures 11(b) and (d), it is concluded that the peak values of transmission occur at different frequencies in the two-layer system and that

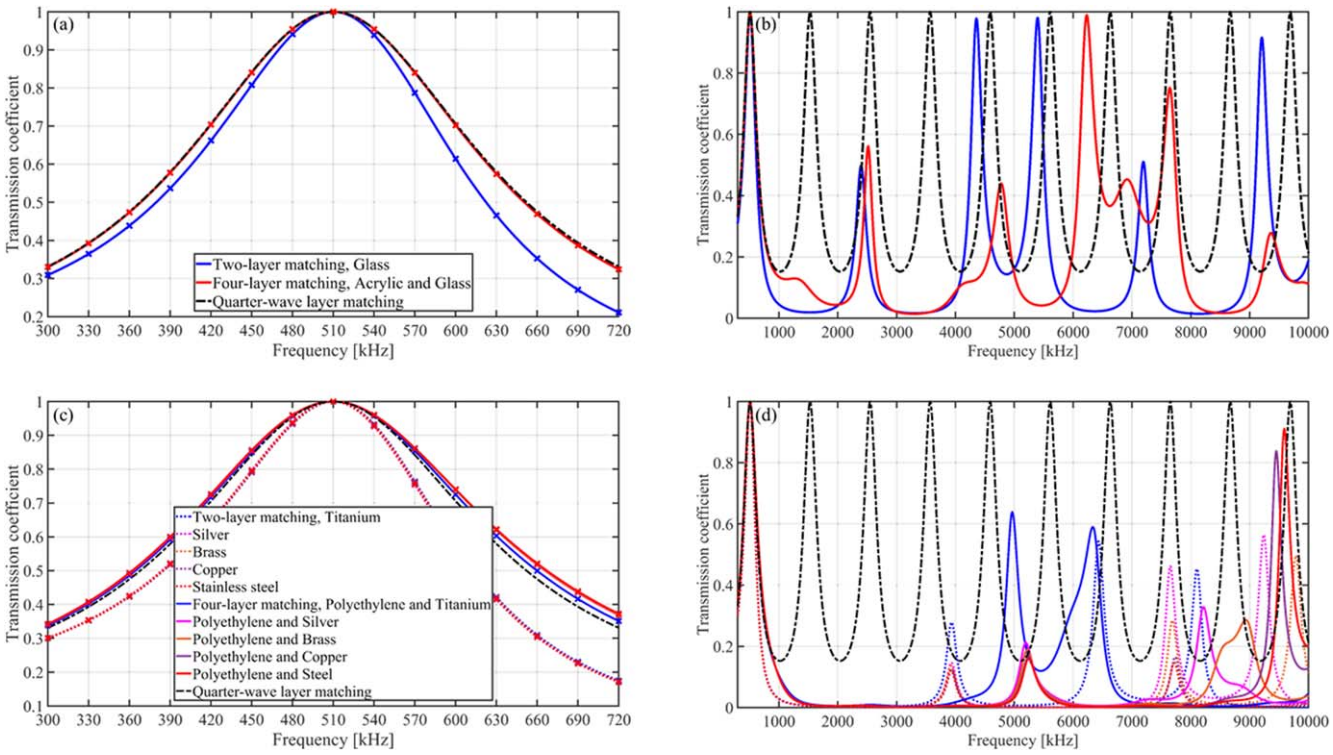

Figure 11. Power transmission coefficient of the matched transducer in the four-layer matching structure using two layers of glue A ($t_2 = t_4 = 0.2$ mm) with two layers of glass and acrylic, compared with the corresponding two-layer and ideal matching system: (a) frequency range from 300–720 kHz, and (b) wider frequency range from 300 kHz–10 MHz. Power transmission coefficient of the matched transducer in the four-layer system using two layers of glue A ($t_2 = t_4 = 0.25$ mm) with the combination of polymer and metal layers, compared with the corresponding two-layer and ideal matching system: (c) frequency range from 300–720 kHz, and (d) wider frequency range from 300 kHz–10 MHz. The legend in (b) and (d) is, respectively, the same as that of (a) and (c).

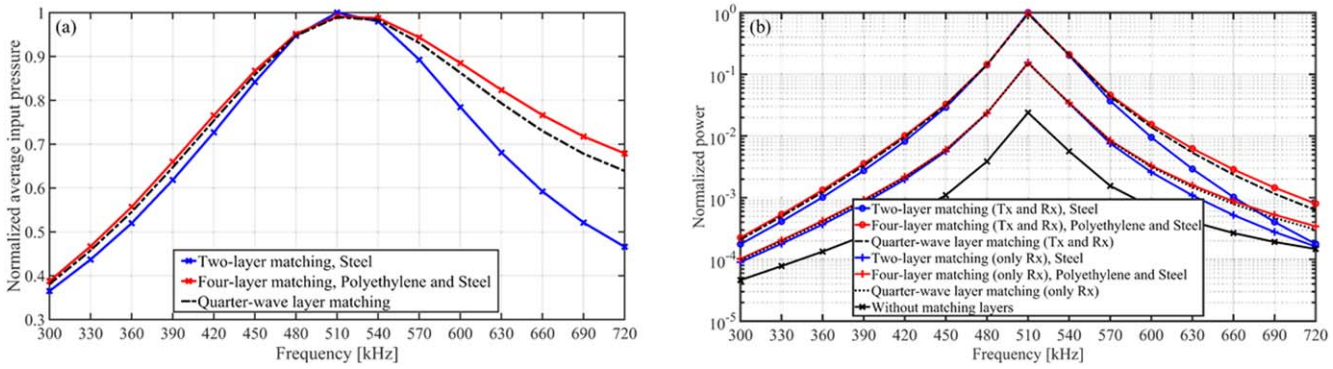

Figure 12. Example of the four-layer system compared with the corresponding two-layer and single quarter-wave matching system using glue C: (a) the average input pressure on the receiver excited by the matched transmitter, and (b) the subsequent electrical power output for the receiver at $d = 60$ mm excited by the acoustic source, analyzed in three scenarios, namely *without matching layers* case depicted with a cross marker, *only Rx* case depicted with plus sign markers, and *Tx and Rx* case depicted with circle markers. The thickness of the glue layers is set to 0.25 mm. The pressure values are obtained using the same experimentally measured pressure fields explained in section 3.3. The dashed-dot and dotted lines in (b), respectively, represent *Tx and Rx* case and *only Rx* case using glue C.

smoother curves of transmission are generated in comparison to those of the four-layer systems. A list of analyzed materials for the four-layer matching system with their determined thicknesses at 510 kHz is presented in table C3 of appendix C.

Figure 12(a) shows the average input pressure on the receiver surface considering an example of the analyzed four-layer material choices, implementing two layers of polyethylene and steel with the two layers of glue A in comparison to that of the two-layer system of using steel and glue A. Consistently, the input acoustic pressure increases for the off-resonance driving frequencies, particularly for the system excited above the fundamental resonance of the transducer, which in turn leads to a considerable power augmentation, as illustrated in figure 12(b). However, due to the stronger attenuation effects using four layers, slightly

higher input pressure and hence higher power enhancements are achieved at 510 kHz in the two-layer structure. Briefly, the foremost objective in the UPT-matching technique is the construction of wide-bandwidth transducers that can greatly transmit the acoustic energy at or near the desired resonant frequency, which is satisfactorily achieved by implementing the two-layer acoustically matching system. In conclusion, adding the number of layers, which subsequently requires more than one layer of glue, is not a practical and efficient solution since the fabrication of transducers with four or more material layers and maintaining the required thicknesses can be extremely difficult, time-consuming and costly.

4. Conclusions

Contactless ultrasonic power transfer (UPT) is a new technology with broad applications, e.g., to support distributed automotive sensing in the automobile industry and wireless networks in biomedical sensors. Current UPT systems suffer from significant acoustic losses through the transmission line from a piezoelectric transmitter to an acoustic medium (e.g., water or human tissue) and then to a piezoelectric receiver. This is due to the acoustic impedance mismatch between the PZT (lead zirconate titanate) transducers and the medium, which causes a narrow transducer bandwidth and a considerable reflection of the acoustic pressure waves at the boundary layers. We investigated the implementation of acoustic impedance matching layers deposited on the front leading surface of the source and receiver transducers to enhance the acoustic power transmission into the medium and then reinforce the input as an excitation into the receiver. A transfer matrix method was used to determine the thicknesses of selected materials in the two-layer matching structure, where one of the layers is the glue and the calculated thicknesses are different from the quarter of materials' wavelength. Subsequently, an electro-elastic model was employed to couple the properties of PZT transmitter and receiver with multiple matching layers and a single classical quarter-wave layer. A design platform was developed that can simplify the construction of acoustically matched transducers, that is, the materials selection and determination of their thicknesses. Simulations were performed to evaluate the electrical power output enhancement in UPT using the two-layer system to match the transducers to water at the resonant frequency. Different material types were selected as the first layer including mainly metals and polymers. The input acoustic pressure on the receiver was determined via the angular spectrum approach using the experimentally measured transmitter output pressure distribution. The ultrasonic material losses were also accounted for in the simulations to accurately quantify the advantages of matching layers in UPT, which is specifically important in lossy acoustic media such as human tissue. The results indicate dramatic electrical power output improvements when implementing matching layers in the UPT system. We also concluded that using more than two layers in the matching structure is not advantageous because it does not lead to a power enhancement at the resonant frequency or to the generation of a noticeably wider frequency bandwidth.

Acknowledgments

This work was supported by the National Science Foundation (NSF) Grant NO. ECCS-1711139, which is gratefully acknowledged.

Appendix A. Measured electrical impedance

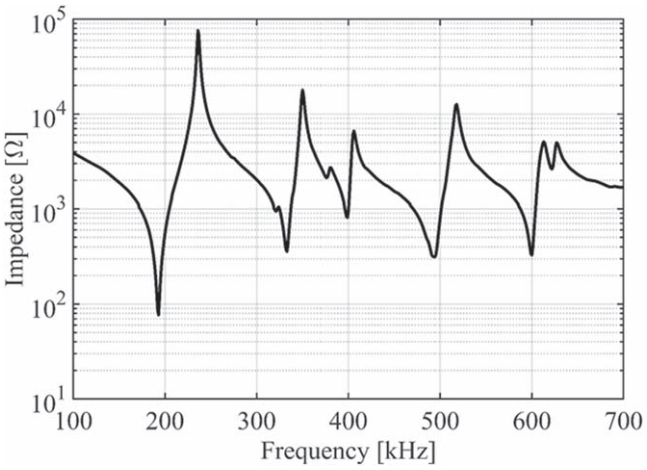

Figure A1. Measured electrical impedance of the unloaded APC850 PZT disk in air using the HP4192A impedance analyzer.

Appendix B. Acoustic radiation impedance

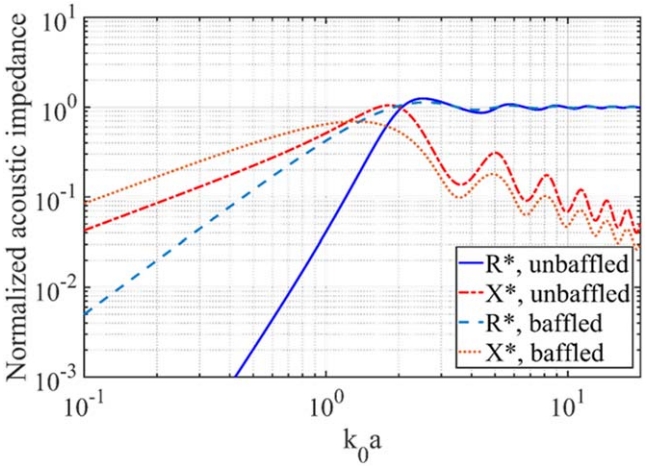

Figure B1. Normalized acoustic radiation resistance $R^* = R_r/(\rho_0 c_0 A)$ and reactance $X^* = X_r/(\rho_0 c_0 A)$ for $1 \leqslant ka \leqslant 20$ of an unbaffled and a baffled piston. c_0 and k_0 are, respectively, the speed of sound and wave number in the acoustic medium (water), and ρ_0 is the density of the medium. Calculations for the unbaffled case is performed with $M = 40$ and $b = a$ (see equations (56) and (57) in [59]).

Appendix C. Materials used in the acoustically matching technique

Table C1. Acoustic properties and calculated thicknesses (at 510 kHz) of the first type of materials used in the two-layer matching system. The attenuation coefficient of glue is taken as 173 Np m^{-1} [79] (measured at 4 MHz). The properties are extracted from [56], unless otherwise mentioned.

Material for ML-1	Characteristic impedance [MRayl]	Sound speed [m s^{-1}]	t_1 [mm]	t_2 (glue A) [mm]	Attenuation coefficient [Np m^{-1}]
Brick	7.4	4300	2.004	0.025	11.5 @ 100 kHz [83]
Concrete	8	3100	1.1	0.138	40.3 @ 510 kHz [84]
Marble	10.5	3800	0.858	0.25	21 @ 510 kHz [85]
Glass	11.1	4910	1.03	0.261	1.15 @ 2 MHz [78]
Porcelain	13.5	5900	0.972	0.290 355	1.15 @ 2 MHz [78]
Slate	13.5	4500	0.742	0.290 355	
Quartz	15.3	5750	0.82	0.303	10.8 @ 450 MHz [86]
Aluminum	17.33	6420	0.797	0.312	1.15 @ 2 MHz [78]
Indium	18.7	2560	0.293	0.316	
Silicon	19.7	8430	0.911	0.318	23 @ 286 MHz [87]
Lead Metaniobate	20.5	3300	0.342	0.32	
Bismuth	21.5	2200	0.216	0.322	
Beryllium	24.1	12 890	1.125	0.326 04	
Tin	24.2	3300	0.287	0.3262	
Lead	24.6	2200	0.188	0.327	
Boron carbide	26.4	11 000	0.873	0.3285	
Granite	26.8	6500	0.508	0.3289	
Thorium	27.12	2400	0.185	0.329	
Titanium	27.3	6100	0.468	0.3293	1.15 @ 2 MHz [78]
Zinc	29.6	4200	0.296	0.331 05	
Zirconium	30.1	4650	0.322	0.3314	
Potassium Sodium Niobate (PSN)	31	6940	0.467	0.332	
Lithium Niobate	33	7080	0.446	0.333	
PZT 5H	33	4440	0.28	0.333	
Cast Iron	33.2	4600	0.288	0.333 05	
Silicon Nitride	36	11 000	0.634	0.334	
Murata PZT	37.5	4720	0.261	0.3347	
Silver	38	3600	0.197	0.334 86	
Brass	40.6	4700	0.24	0.3356	
Niobium	42.2	4920	0.241	0.335 95	
Titanium Carbide	42.6	8270	0.402	0.336 04	
Zircaloy	44.2	4720	0.221	0.336 37	
Copper	44.6	5010	0.232	0.3364	
Stainless Steel	45.7	5790	0.262	0.3366	
Iron	46.4	5900	0.263	0.3368	
Inconel	47.2	5700	0.25	0.3369	
Nickel	49.5	5600	0.234	0.3372	
Uranium	63	3400	0.111	0.338 527	
Molybdenum	63.1	6300	0.206	0.338 534	
Gold	63.8	3240	0.105	0.338 58	
Tantalum	68.06	4100	0.124	0.339	
Platinum	69.8	3260	0.096	0.3389	
Silicon Carbide	91.8	6660	0.149	0.3396	
Tungsten	101	5200	0.106	0.3398	1.15 @ 2 MHz [78]

Table C2. Acoustic properties and calculated thicknesses (at 510 kHz) of the second type of materials used in the two-layer matching system. The attenuation coefficient of glue is taken as 173 Np m^{-1} [79] (measured at 4 MHz). The properties are extracted from [56], unless otherwise mentioned.

Material for ML-1	Characteristic impedance [MRayl]	Sound speed [m s^{-1}]	t_1 [mm]	t_2 (glue B) [mm]	Attenuation coefficient [Np m^{-1}]
Clear Polycarbonate	2.69	2270	0.994	0.706	
Parylene-C	2.7 [26]	2200 [26]	0.957	0.704	3570 @ 100 MHz [26]
Polycarbonate (Lexan)	2.75	2300	0.975	0.694	267.1 @ 5 MHz
Polysulfone (PSO)	2.78	2240	0.937	0.689	48.9 @ 2 MHz
Parylene-N	2.85 [26]	2100 [26]	0.856	0.678	1496 @ 100 MHz [26]
Nylon	2.9	2600	1.044	0.671	33.4 @ 5 MHz
Oak Wood	2.9	4000	1.606	0.671	
Teflon	2.97	1390	0.548	0.662	
Mylar	3	2540	0.994	0.659	2000 @ 50 MHz [88]
Clear Acrylic	3.26	2750	1.03	0.63	73.7 @ 5 MHz
PVC	3.27	2380	0.89	0.629	
PVDF	3.43 [57]	1930 [57]	0.709	0.613	154.3 @ 1 MHz [82]
Polyimide	3.6 [26]	2430 [26]	0.88	0.597	646.4 @ 100 MHz [26]
Bakelite	3.63	1590	0.575	0.595	
Pressed Graphite	4.1	2400	0.852	0.552	39.4 @ 1 MHz [89]
Melopas	4.93	2900	1.035	0.476	82.9 @ 2.5 MHz
Vitreous Carbon	6.26	4260	1.644	0.327	311 @ 50 MHz[a] [90]
Pyrolytic Carbon	7.31	3310	1.526	0.085	39.4 @ 1 MHz[b] [89]

[a] The attenuation coefficient of vitreous carbon is assumed to be the same as that of hard carbon.
[b] The attenuation coefficient of pyrolytic carbon is assumed to be the same as that of graphite.

Table C3. Calculated thicknesses (at 510 kHz) of materials used in the four-layer matching system. Characteristic impedance, sound speed, and attenuation coefficient of polyethylene are, respectively, 2.33 MRayl [56], 2430 m s^{-1} [56], and 38 Np m^{-1} [57] (measured at 2 MHz).

Material for ML-3	t_1 (Clear Acrylic) [mm]	t_2 (glue A) [mm]	t_3 [mm]	t_4 (glue A) [mm]
Glass	0.28	0.2	1.031	0.2
Material for ML-3	t_1 (Polyethylene) [mm]	t_2 (glue A) [mm]	t_3 [mm]	t_4 (glue A) [mm]
Titanium	0.482	0.25	0.506	0.25
Silver	0.522	0.25	0.217	0.25
Brass	0.527	0.25	0.266	0.25
Copper	0.534	0.25	0.2586	0.25
Stainless Steel	0.535	0.25	0.292	0.25

Appendix D. Ultrasonic material attenuation variations with frequency

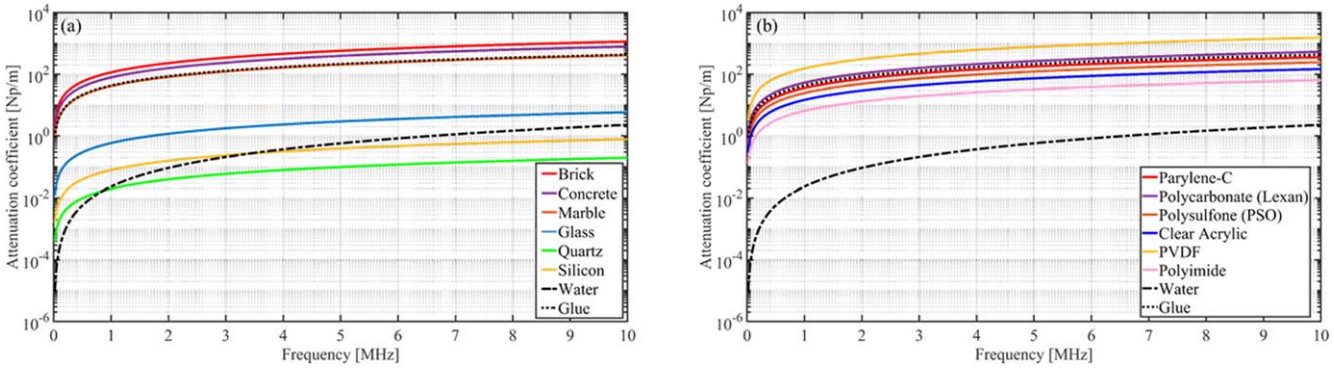

Figure D1. Ultrasonic attenuation versus frequency for the materials analyzed in the electrical power calculations compared with that of used glue and water: (a) first material type, and (b) second material type. The variations of the attenuation with frequency for some of the analyzed materials are not presented due to the close similarity of the attenuation values with the one shown in the figure (see appendix C for other materials' attenuation coefficient value).

ORCID iDs

Marjan Bakhtiari-Nejad https://orcid.org/0000-0003-0517-0335
Shima Shahab https://orcid.org/0000-0003-1970-5345

References

[1] Shahab S and Erturk A 2014 Contactless ultrasonic energy transfer for wireless systems: acoustic-piezoelectric structure interaction modeling and performance enhancement *Smart Mater. Struct.* **23** 125032
[2] Shahab S, Gray M and Erturk A 2015 Ultrasonic power transfer from a spherical acoustic wave source to a free-free piezoelectric receiver: modeling and experiment *J. Appl. Phys.* **117** 104903
[3] Ishiyama T, Kanai Y, Ohwaki J and Mino M 2003 Impact of a wireless power transmission system using an ultrasonic air transducer for low-power mobile applications *IEEE Symp. on Ultrasonics (Honolulu, HI)* (https://doi.org/10.1109/ultsym.2003.1293157)
[4] Roes M, Hendrix M and Duarte J 2011 Contactless energy transfer through air by means of ultrasound *IECON 37th Annual Conf. of the IEEE Industrial Electronics Society (Melbourne)* (https://doi.org/10.1109/iecon.2011.6119486)
[5] Ozeri S and Shmilovitz D 2010 Ultrasonic transcutaneous energy transfer for powering implanted devices *Ultrasonics* **50** 556–66
[6] Meng M and Kiani M 2017 Design and optimization of ultrasonic wireless power transmission links for millimeter-sized biomedical implants *IEEE Trans. Biomed. Circuits Syst.* **11** 98–107
[7] Lawry T J, Wilt K R, Ashdown J D, Scarton H A and Saulnier G J 2012 A high-performance ultrasonic system for the simultaneous transmission of data and power through solid metal barriers *IEEE Trans. Ultrason. Ferroelectr. Freq. Control* **60** 194–203
[8] Yang D-X, Hu Z, Zhao H, Hu H-F, Sun Y-Z and Hou B-J 2015 Through-metal-wall power delivery and data transmission for enclosed sensors: a review *Sensors* **15** 31581–605
[9] Roes M G, Duarte J L, Hendrix M A and Lomonova E A 2013 Acoustic energy transfer: a review *IEEE Trans. Ind. Electron.* **60** 242–8
[10] Ozeri S and Shmilovitz D 2014 Simultaneous backward data transmission and power harvesting in an ultrasonic transcutaneous energy transfer link employing acoustically dependent electric impedance modulation *Ultrasonics* **54** 1929–37
[11] Bhargava A and Shahab S 2019 Coupling of nonlinear shape memory polymer cantilever dynamics with focused ultrasound field *Smart Mater. Struct.* (https://doi.org/10.1088/1361-665X/ab0b71)
[12] Bakhtiari-Nejad M, Elnahhas A, Hajj M R and Shahab S 2018 Acoustic holograms in contactless ultrasonic power transfer systems: modeling and experiment *J. Appl. Phys.* **124** 244901
[13] Bakhtiari-Nejad M, Elnahhas A, Hajj M R and Shahab S 2018 Passive metamaterial-based acoustic holograms in ultrasound energy transfer systems *Proc. SPIE* **10595** 1059518
[14] Meesala V C, Hajj M R and Shahab S 2019 Modeling and identification of electro-elastic nonlinearities in ultrasonic power transfer systems *Nonlinear Dyn.* **99** 249–68
[15] Goll J H and Auld B A 1975 Multilayer impedance matching schemes for broadbanding of water loaded piezoelectric transducers and high Q electric resonators *IEEE Trans. Sonics Ultrason.* **22** 52–3
[16] Inoue T, Ohta M and Takahashi S 1987 Design of ultrasonic transducers with multiple acoustic matching layers for medical application *IEEE Trans. Ultrason. Ferroelectr. Freq. Control* **34** 8–16
[17] Thiagarajan S, Martin R W, Proctor A, Jayawadena I and Silverstein F 1997 Dual layer matching (20 MHz) piezoelectric transducers with glass and parylene *IEEE Trans. Ultrason. Ferroelectr. Freq. Control* **44** 1172–4
[18] Persson H and Hertz C 1985 Acoustic impedance matching of medical ultrasound transducers *Ultrasonics* **23** 83–9
[19] Shung K K and Zippuro M 1996 Ultrasonic transducers and arrays *IEEE Eng. Med. Biol. Mag.* **15** 20–30
[20] Kossoff G 1966 The effects of backing and matching on the performance of piezoelectric ceramic transducers *IEEE Trans. Sonics Ultrason.* **13** 20–30
[21] Desilets C S, Fraser J D and Kino G S 1978 The design of efficient broad-band piezoelectric transducers *IEEE Trans. Sonics Ultrason.* **25** 115–25
[22] Souquet J, Defranould P and Desbois J 1979 Design of low-loss wide-band ultrasonic transducers for noninvasive medical application *IEEE Trans. Sonics Ultrason.* **26** 75–80
[23] Goll J H 1979 The design of broad-band fluid-loaded ultrasonic transducers *IEEE Trans. Sonics Ultrason.* **26** 385–93
[24] Beerman H P 1981 Optimizing matching layers for a three-section broad-band piezoelectric PZT-5A transducer operating into water *IEEE Trans. Sonics Ultrason.* **28** 52–3
[25] Xu Q, Madhavan C, Srinivasan T, Yoshikawa S and Newnham R 1988 Composite transducer with multiple piezoelectric matching layers *IEEE Ultrasonics Symp. Proc. (Chicago, IL)* (https://doi.org/10.1109/ultsym.1988.49429)
[26] Hadimioglu B and Khuri-Yakub B 1990 Polymer films as acoustic matching layers *IEEE Symp. on Ultrasonics (Honolulu, HI)* (https://doi.org/10.1109/ultsym.1990.171581)
[27] Kim Y-B and Roh Y 1998 New design of matching layers for high power and wide band ultrasonic transducers *Sens. Actuators, A* **71** 116–22
[28] Rhee S, Ritter T, Shung K, Wang H and Cao W 2001 Materials for acoustic matching in ultrasound transducers *IEEE Ultrasonics Symp. Proc. (Cat. No.01CH37263) (Atlanta, GA)* (https://doi.org/10.1109/ultsym.2001.991900)
[29] Gudra T and Opieliński K J 2002 Influence of acoustic impedance of multilayer acoustic systems on the transfer function of ultrasonic airborne transducers *Ultrasonics* **40** 457–63
[30] Álvarez-Arenas T G 2004 Acoustic impedance matching of piezoelectric transducers to the air *IEEE Trans. Ultrason. Ferroelectr. Freq. Control* **51** 624–33
[31] Gudra T and Banasiak D 2018 Methods for selecting multicomponent layers which match the acoustic impedance of ultrasound transducers to various media *Joint Conf. Acoustics (Ustka)* (https://doi.org/10.1109/acoustics.2018.8502416)
[32] Guo F, Wang Y, Huang Z, Qiu W, Zhang Z, Wang Z, Dong J, Yang B and Cao W 2018 Magnesium alloy matching layer for PMN-PT single crystal transducer applications *IEEE Trans. Ultrason. Ferroelectr. Freq. Control* **65** 1865–72
[33] Ke Q, Liew W H, Tao H, Wu J and Yao K 2019 KNNS-BNZH lead-free 1–3 piezoelectric composite for ultrasonic and photoacoustic imaging *IEEE Trans. on Ultrasonics, Ferroelectrics, and Frequency Control* **66** 1395–1401
[34] Toda M and Thompson M 2010 Novel multi-layer polymer-metal structures for use in ultrasonic transducer impedance matching and backing absorber applications *IEEE Trans. Ultrason. Ferroelectr. Freq. Control* **57** 2818–27
[35] Toda M and Thompson M 2012 Detailed investigations of polymer/metal multilayer matching layer and backing absorber structures for wideband ultrasonic transducers

IEEE Trans. Ultrason. Ferroelectr. Freq. Control **59** 231–42
[36] Brown J A, Sharma S, Leadbetter J, Cochran S and Adamson R 2014 Mass-spring matching layers for high-frequency ultrasound transducers: a new technique using vacuum deposition *IEEE Trans. Ultrason. Ferroelectr. Freq. Control* **61** 1911–21
[37] Gorostiaga M, Wapler M and Wallrabe U 2015 Novel spring-mass matching layer fabrication *IEEE Int. Ultrasonics Symp. (IUS) (Taipei)* (https://doi.org/10.1109/ultsym.2015.0366)
[38] Opieliński K J and Gudra T 2002 Influence of the thickness of multilayer matching systems on the transfer function of ultrasonic airborne transducer *Ultrasonics* **40** 465–9
[39] Assaad J, Ravez M and Bruneel C 1996 Application of the finite-element method for modeling backed transducers *J. Acoust. Soc. Am.* **100** 3098–103
[40] Callens D, Bruneel C and Assaad J 2004 Matching ultrasonic transducer using two matching layers where one of them is glue *Ndt & E International* **37** 591–6
[41] Hill R and El-Dardiry S M 1980 A theory for optimization in the use of acoustic emission transducers *J. Acoust. Soc. Am.* **67** 673–82
[42] Lockwood G R and Foster F S 1994 Modeling and optimization of high-frequency ultrasound transducers *IEEE Trans. Ultrason. Ferroelectr. Freq. Control* **41** 225–30
[43] Wilcox P, Monkhouse R, Cawley P, Lowe M and Auld B 1998 Development of a computer model for an ultrasonic polymer film transducer system *NDT & E International* **31** 51–64
[44] Basaeri H, Christensen D B and Roundy S 2016 A review of acoustic power transfer for biomedical implants *Smart Mater. Struct.* **25** 123001
[45] Hu Y-C, Liao P-L, Shih W-P, Wang X-Y and Chang P-Z 2009 Study on the acoustic impedance matching of human tissue for power transmitting/charging system of implanted biochip *2009 IEEE 3rd Int. Conf. on Nano/Molecular Medicine and Engineering (Tainan)* (IEEE) (https://doi.org/10.1109/nanomed.2009.5559087)
[46] Denisov A and Yeatman E 2010 Ultrasonic versus inductive power delivery for miniature biomedical implants *2010 Int. Conf. on Body Sensor Networks (Singapore)* (https://doi.org/10.1109/bsn.2010.27)
[47] Song S H, Kim A and Ziaie B 2015 Omnidirectional ultrasonic powering for millimeter-scale implantable devices *IEEE Trans. Biomed. Eng.* **62** 2717–23
[48] Christensen D B and Roundy S 2018 Non-dimensional analysis of depth, orientation, and alignment in acoustic power transfer systems *Smart Mater. Struct.* **27** 125013
[49] Ozeri S, Shmilovitz D, Singer S and Wang C-C 2010 Ultrasonic transcutaneous energy transfer using a continuous wave 650 kHz Gaussian shaded transmitter *Ultrasonics* **50** 666–74
[50] Seo D, Carmena J M, Rabaey J M, Alon E and Maharbiz M M 2013 Neural dust: an ultrasonic, low power solution for chronic brain-machine interfaces (arXiv:1307.2196)
[51] Guillermic R-M, Lanoy M, Strybulevych A and Page J H 2019 A PDMS-based broadband acoustic impedance matched material for underwater applications *Ultrasonics* **94** 152–7
[52] Kunkel H, Locke S and Pikeroen B 1990 Finite-element analysis of vibrational modes in piezoelectric ceramic disks *IEEE Trans. Ultrason. Ferroelectr. Freq. Control* **37** 316–28
[53] Guo N, Cawley P and Hitchings D 1992 The finite element analysis of the vibration characteristics of piezoelectric discs *J. Sound Vib.* **159** 115–38
[54] Gorostiaga M, Wapler M and Wallrabe U 2017 Analytic model for ultrasound energy receivers and their optimal electric loads II: experimental validation *Smart Mater. Struct.* **26** 105021
[55] Kinsler L E, Frey A R, Coppens A B and Sanders J V Dec 1999 *Fundamentals of Acoustics, Fourth Edition* (New York: Wiley)
[56] Selfridge A R 1985 Approximate material properties in isotropic materials *IEEE Trans. Sonics Ultrason.* **32** 381–94
[57] Mark J E 2006 *Physical Properties of Polymers Handbook, Second Edition* (New York: Springer)
[58] Rao S S 2007 *Vibration of Continuous Systems* (Hoboken, NJ: Wiley) (https://doi.org/10.1002/9780470117866)
[59] Mellow T and Kärkkäinen L 2005 On the sound field of an oscillating disk in a finite open and closed circular baffle *J. Acoust. Soc. Am.* **118** 1311–25
[60] Butler J L and Sherman C H 2007 *Transducers and Arrays for Underwater Sound* (New York: Springer) (https://doi.org/10.1007/978-0-387-33139-3)
[61] Erturk A and Inman D J 2011 *Piezoelectric Energy Harvesting* (Chichester: Wiley) (https://doi.org/10.1002/9781119991151)
[62] Jacobsen F, Moreno-Pescador G, Fernandez-Grande E and Hald J 2011 Near field acoustic holography with microphones on a rigid sphere (L) *J. Acoust. Soc. Am.* **129** 3461–4
[63] Sapozhnikov O A, Tsysar S A, Khokhlova V A and Kreider W 2015 Acoustic holography as a metrological tool for characterizing medical ultrasound sources and fields *J. Acoust. Soc. Am.* **138** 1515–32
[64] Maynard J D, Williams E G and Lee Y 1985 Nearfield acoustic holography: I. Theory of generalized holography and the development of NAH *J. Acoust. Soc. Am.* **78** 1395–413
[65] Veronesi W and Maynard J D 1987 Nearfield acoustic holography (NAH) II. Holographic reconstruction algorithms and computer implementation *J. Acoust. Soc. Am.* **81** 1307–22
[66] Williams E G 1999 *Fourier Acoustics: Sound Radiation and Nearfield Acoustical Holography* (Cambridge: Academic) (https://doi.org/10.1016/B978-0-12-753960-7.X5000-1)
[67] Kim A, Zhou J, Samaddar S, Song S H, Elzey B D, Thompson D H and Ziaie B 2019 An implantable ultrasonically-powered micro-light-source (μLight) for photodynamic therapy *Sci. Rep.* **9** 1395
[68] Whitworth G 2001 Discussion of 1D piezoelectric transducer models with loss *IEEE Trans. Ultrason. Ferroelectr. Freq. Control* **48** 844–6
[69] Gorostiaga M, Wapler M and Wallrabe U 2017 Analytic model for ultrasound energy receivers and their optimal electric loads *Smart Mater. Struct.* **26** 085003
[70] https://americanpiezo.com/
[71] https://americanpiezo.com/apc-materials/piezoelectric-properties.html
[72] Melde K, Mark A G, Qiu T and Fischer P 2016 Holograms for acoustics *Nature* **537** 518
[73] Davis J R 2003 *Handbook of Materials for Medical Devices* (Materials Park, OH: ASM International)
[74] Krimholtz R, Leedom D A and Matthaei G L 1970 New equivalent circuits for elementary piezoelectric transducers *Electron. Lett.* **6** 398–9
[75] Gorostiaga M, Wapler M and Wallrabe U 2018 Optimizing piezoelectric receivers for acoustic power transfer applications *Smart Mater. Struct.* **27** 075024
[76] Castillo M, Acevedo P and Moreno E 2003 KLM model for lossy piezoelectric transducers *Ultrasonics* **41** 671–9
[77] Liu D-L and Waag R C 1997 Propagation and backpropagation for ultrasonic wavefront design *IEEE Trans. Ultrason. Ferroelectr. Freq. Control* **44** 1–13
[78] Krautkrämer J and Krautkrämer H 1983 *Ultrasonic Testing of Materials* (Berlin: Springer) (https://doi.org/10.1007/978-3-662-02357-0)

[79] Wilt K, Lawry T, Scarton H and Saulnier G 2015 One-dimensional pressure transfer models for acoustic–electric transmission channels *J. Sound Vib.* **352** 158–73
[80] Wells P N 1999 Ultrasonic imaging of the human body *Rep. Prog. Phys.* **62** 671
[81] Hoskins P R, Martin K and Thrush A 2010 *Diagnostic Ultrasound: Physics and Equipment, Second Edition* (New York: Cambridge University Press) (https://doi.org/10.1017/cbo9780511750885)
[82] Bloomfield P E, Lo W-J and Lewin P A 2000 Experimental study of the acoustical properties of polymers utilized to construct PVDF ultrasonic transducers and the acousto-electric properties of PVDF and P (VDF/TrFE) films *IEEE Trans. Ultrason. Ferroelectr. Freq. Control* **47** 1397–405
[83] Kojima T, Haya H, Minegishi K and Nguyen R T 2008 Ultrasonic velocity measurement for analysis of brick structure *2008 IEEE Ultrasonics Symp. (Beijing)* (https://doi.org/10.1109/ultsym.2008.0098)
[84] Philippidis T and Aggelis D 2005 Experimental study of wave dispersion and attenuation in concrete *Ultrasonics* **43** 584–95
[85] Auberger M and Rinehart J S 1961 Ultrasonic velocity and attenuation of longitudinal waves in rocks *J. Geophys. Res.* **66** 191–9
[86] Lamb J and Richter J 1966 Anisotropic acoustic attenuation with new measurements for quartz at room temperatures *Proc. R. Soc.* A **293** 479–92
[87] Lambade S, Sahasrabudhe G and Rajagopalan S 1995 Temperature dependence of acoustic attenuation in silicon *Phys. Rev.* B **51** 15861
[88] Rajagopal S, Sadhoo N and Zeqiri B 2015 Reference characterisation of sound speed and attenuation of the IEC agar-based tissue-mimicking material up to a frequency of 60 MHz *Ultrasound Med. Biol.* **41** 317–33
[89] Serabian S 1967 Influence of attenuation upon the frequency content of a stress wave packet in graphite *J. Acoust. Soc. Am.* **42** 1052–9
[90] Lasjaunias J, Saint-Paul M, Bilušić A, Smontara A, Gradečak S, Tonejc A, Tonejc A and Kitamura N 2002 Acoustic and thermal transport properties of hard carbon formed from C 60 fullerene *Phys. Rev.* B **66** 014302